

A preliminary analysis of the optical properties of atmosphere in the Millard County region (Utah - USA)

Brian Fick - University of Utah (fick@casa.physics.utah.edu)

John Matthews - University of New Mexico (johnm@lambda.phys.unm.edu)

Paul Sommers - University of Utah (sommers@mail.physics.utah.edu)

Renato Biral - State University of Campinas (biral@ifi.unicamp.br)

Introduction

This work refers to the reduction of the atmospheric horizontal mean free path data in the northern *Pierre Auger Observatory* site, in Millard County (Utah). Basically, the measurement consists in a series of photometric data obtained by CCD cameras that record the signal of two light bulbs placed near the ground during the night. The data acquisition was automated, and covered an almost full year of the apparatus operation.

All the initiatives about the apparatus implementation and operation were took by Brian Fick, site-manager of the northern site of the *Pierre Auger Observatory*, and researcher of the University of Utah.

Description of the used apparatus

On the literature, usually an evaluation of the mean free path is performed during daylightⁱ. However, due the nature of the fluorescence light measurements, a photometric method (more suited for night measurements) was devised.

Two halogen bulbs were placed on a long horizontal optical path inside the intended northern site for the *Pierre Auger Observatory*, in Millard County (Utah). To the photometric measurements were used two CCDs camerasⁱⁱ connected to a remote computer. So, the CCD frame acquisition could be done automatically over a long period of time, and in several occasions during the night, being the frames stored in the computer that managed the CCDs.

The light bulbs localization on the site, as well the CCD cameras localization, is shown in Figure 1. The bulb on the point named “*far site*” (point “a” on the figure) is on a natural elevation named *Cricket Mountains* (250 meters above the ground), on the roof of a AT&T building, powered with electric energy. The bulb on the point designated as “*near site*” (point “b” on the figure) is placed on the “basin” chose to the *Pierre Auger Observatory*, being powered however by a set of batteries charged by solar panels.

ⁱ Middleton, W.E.K., “Visibility in Meteorology” (The University of Toronto Press, Toronto, 1947), chapter 8.

ⁱⁱ The CCD cameras used were two MEADE Pictor XT-Series, model 208 XT (242 rows by 324 columns, 8 bits of gray), attached to an Olympus OM Zuiko 50 mm 1:1.8 lens.

The set “CCDs cameras + acquisition computer” is in a radio retransmission building in the *Cedar Mountain* elevation (point “c” on the figure), 250 meters above the ground and next to the town of Fillmore. The CCDs cameras were placed on the roof of the radio retransmission building, sheltered in a metallic box provided with a glass window. The apparatus (light bulbs, CCD cameras and computer) were just powered during the night, by the use of timers.

The light bulbs of the *near* and *far sites* were placed 15 and 50 km from the CCD cameras, being their positions settled by the use of GPS. The light bulbs were intentionally placed in the same line of sight seen from the *Cedar Mountain* retransmission building, and so each frame shot by the CCDs simultaneously had the images of the two light bulbs (Figure 2).

The nominal intensity of the light bulbs was 20 Watts (for the *near site* bulb) and 35 Watts (for the *far site* bulb), with their emission collimated towards the CCDs direction by the use of a tube. The dynamic range of the used CCDs was of just 256 gray levels (8 bits). As the “ r^{-2} ” geometric factor implied in a flux decrease of 10 times between the two sites, the light sources were equalized by the use of neutral density filters in front of the light bulb placed in the *near site*. The equalization was obtained by the application of a set of Kodak X2 e X4 neutral density filters, providing a final attenuation of 8 times on the light emitted by this bulb.

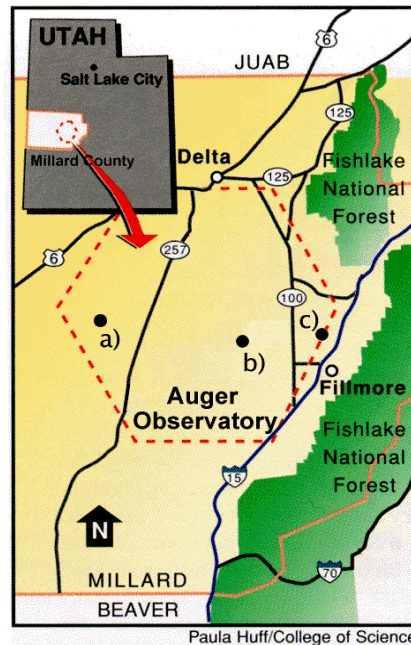


Figure 1: Map of northern site intended for the *Pierre Auger Observatory*, with the localization of the light bulbs and CCD cameras employed in this study (for the complete description, please, refer to the text). The hexagonal array design, as present on the plot, is not representative of the final ground array configuration to be adopted for this site (illustration from the “*Science Spotlight*” bulletin, a publication of the *University of Utah’s College of Science* (vol. 2, page 26)).



Figure 2: Picture from the radio retransmission building on the *Cedar Mountain* (shot during a full moon night), showing the light bulb placed on the *far site* (topmost light point, on the *Crickets Mountains*, 50 km away), and the light bulb placed on the *near site* (point of light just below and to the left, 15 km away). The mountain behind the *Crickets Mountains* (on the horizon, to the right) is 70-80 km away, illustrating the exceptional atmospheric transparency of this site.

The limited range of grays in the CCD recording provided a further overcome: usually the light bulb images laid “pin pointed” in a couple of saturated pixels, being just the background value recorded by their neighboring pixels. In order to avoid a dependence of just a few of the pixels in the CCDs, the images were intentionally defocused, spreading the light bulb signal on a wider CCD area.

In the present study it was also tried a simultaneous photometry of the light source in two different wavelength ranges. This was achieved by the use of two different CCDs cameras (from now on denominated “CCD A” and “CCD B”). The CCD A had a Kodak Wratten filter W47b (centered in 430 nm, “blue” range) in front of it, and the CCD B had a Kodak Wratten filter W58 (centered in 530 nm, “green” range) in front of it (Figure 3). The measurements of the “blue” mean free path would provide us a more representative evaluation of the ultraviolet fluorescence light emitted by atmospheric showers. On the other hand, measurements of the “green” mean free path would be more representatives of visual evaluations of “*Meteorological Range*”, parameter used as input by sophisticated atmospheric evaluation codes, as the widely known MODTRANⁱⁱⁱ. As a matter of fact, measurements of the *Meteorological Range* could be correlated a naked eye evaluations such as the *Visibility*^{iv}.

The Kodak Wratten filters are transparent in the infrared region, where the CCD element has it maximum sensibility. To avoid the infrared light contamination, it was placed a Kodak “*Infrared Cutoff*” filter just ahead each CCD element (Figure 3).

ⁱⁱⁱ Berk. A., Bermstein L.S., Robertson D.C. , “MODTRAN: A moderate resolution model for LOWTRAN 7 ”. GL-TR-89-0122 (1989)

^{iv} Gordon, J.I. , “Daytime Visibility, A Conceptual Review”. AFGL-TR-79-0257, AD-A085451 (1979) ; Duntley S.Q., Gordon J.I., Taylor J.H., White C.T., Boileau, A.R., Tyler, J.E., Austin R.W., Harris, J.L. , “Visibility”. *Applied Optics* **3**, page 549-602 (1964)

In every night it was taken three sequences of CCD pictures, for both CCDs, typically at 10 PM, 1 AM and 4 AM. In order to minimize several of the intrinsic fluctuations of the method, each sequence of pictures was a set of 10 CCD “photos”, shot first with the “blue” CCD (CCD A), and then with the “green” CCD (CCD B).

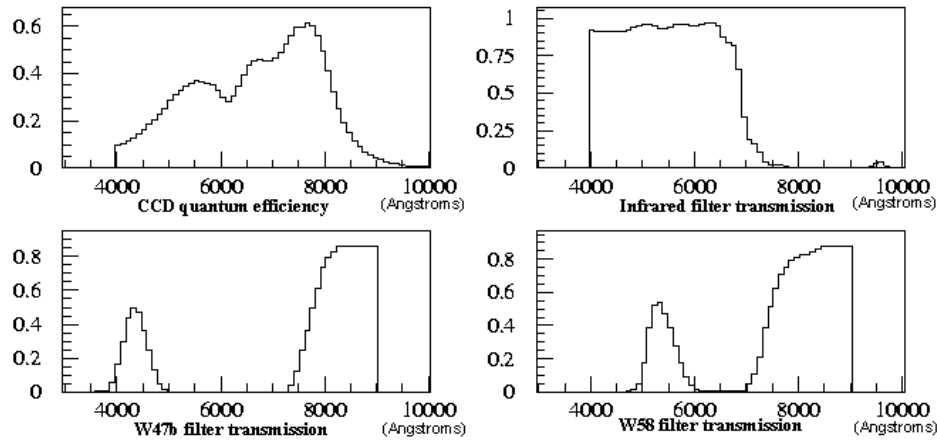


Figure 3: Spectral efficiency of the several components of the photometric apparatus, following the manufacturer curves.

The MODTRAN code, and the attenuation mean free path in the atmosphere

For a good data reduction of a cosmic ray fluorescence light experiment, it is required a good modeling of the atmospheric properties present in each particular night. However, thorough atmospheric profiles are difficult to obtain and, for this reason, often an atmospheric semi-empirical model is employed.

One of the best atmospheric codes available, regarded the optical properties of the atmosphere, is the MODTRAN 3. This code was developed by the American Air Force Laboratories, being used as to civil than to military purposes.

In order to a proper selection of the vertical profile from an atmospheric model, it is required an initial assumption of the latitude range and weather season representative of the site conditions. An assumption of the vertical aerosol profile and composition on atmosphere is of utmost importance in evaluations as intended in our studies. A changing of the individual gas contents of the atmospheric envelope can be easily provided, as it proves be necessary.

Referred to the light attenuation evaluation, one of the MODTRAN most representative input parameters is the *Meteorological Range*, related directly to the

horizontal mean free path of visible light near the ground. The *Meteorological Range* can be described as^v

$$(\text{Meteorological Range}) = \frac{3.912}{\beta_{tot}} = 3.912 * \lambda \text{ (km)}$$

where “ β_{tot} ” is the extinction coefficient (in km^{-1}), and “ λ ” is the attenuation mean free path of visible light in the atmosphere.

The attenuation mean free path measured into the visible range is function of two dominant phenomena: the Rayleigh scattering (scattering due molecules) and the Mie scattering (scattering due aerosols). Other attenuation sources, like light absorption by molecules, can be considered secondary inside the visible spectral range. The same can be stated to light absorption of light due aerosol, unless in the case of heavy polluted atmospheres.

Remembering that “optical thickness” (“ τ ”) can be written as

$$\frac{I}{I_0} = \exp(-\beta_{tot}x) = \exp(-x / \lambda) = \exp(-\tau) ,$$

we have, to several MODTRAN 3 initial atmospheric conditions, the results presented in the Figure 4.

A better knowledge of the MODTRAN input parameters would provide us a better vertical atmospheric attenuation profile. So, the apparatus photometric data could be use to provide a better selection of representative input parameters to an atmospheric modeling code as MODTRAN. A constant atmosphere monitoring and a better knowledge of the atmospheric properties are fundamental to the proper correlation between the received fluorescence photons and the estimated number of charged particles present in an atmospheric shower.

Description of the employed analysis and calibration

When considering an isotropic light source with intensity^{vi} “ I_o ”, placed at a distance “ r ” from the observer and in a **non** absorptive media, the light irradiance “ S ” received could be written as

$$S = I_0 r^{-2}$$

but, in the presence of some kind of uniform and constant attenuation, the expression can be re-written as

^v Earl J. McCartney, “Optics of the Atmosphere (Scattering by Molecules and Particles)”. John Wiley & Sons (1976), page 42

^{vi} More precisely “radiant flux” (provided, for example, in *Watts*)

$$S = \frac{I_0}{r^2} \exp(-r/\lambda)$$

where “ λ ” is the mean free path, representative for a narrow range of wavelengths (the so-called Bouguer-Lambert law^{vii}).

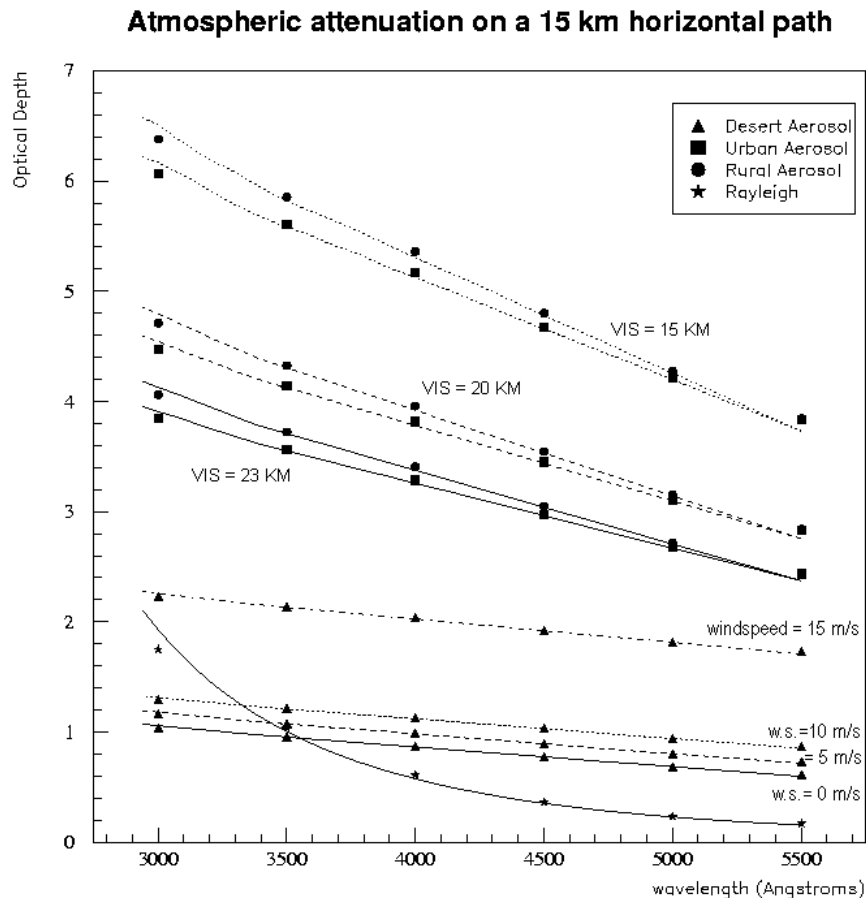


Figure 4: Optical thickness obtained with the MODTRAN 3, to a horizontal optical path of 15 km, to several meteorological conditions.

In a photometric evaluation, usually the “ I_o ” value of the light source is assumed unknown. A proper evaluation of “ I_o ” could be performed, for example, splitting the source light beam into a calibration device near the source.

In this present evaluation, it was used two distinct light sources, with intensity “ I_1 ” and “ I_2 ”. Their values are assumed unknown but, assuming a uniform path between the observer and both light sources, the light mean free path could be given by the rate between the irradiances measured by the CCDs, “ S_1 ” and “ S_2 ”, by the following the expression

^{vii} In really, with the geometric “ r^{-2} ” factor, the expression is known as Allard’s law

$$\lambda = \frac{(r_2 - r_1)}{\ln\left(\frac{S_1 \left(\frac{r_1^2}{r_2^2}\right) I_2}{S_2 \left(\frac{r_2^2}{r_1^2}\right) I_1}\right)}$$

The values for “ r_1 ” e “ r_2 ” are known, and the irradiances “ S_1 ” and “ S_2 ” are measured and stored in the hard disk over the nights. Despite the knowledge of the nominal values of the power of the light bulbs used, the relationship “ I_2/I_1 ” is, *a priori*, unknown. This relationship must be measured by a calibration procedure.

To the experiment calibration it was used a third, roving light source. The intensities “ S_1^{std} ” and “ S_2^{std} ” were measured as the roving light was positioned on the place of the *near* and *far* lights respectively.

The calibration measurements were taken together with the light irradiance of the *near* and *far* lights irradiances at the same night, under the same conditions (“ S_1' ” and “ S_2' ”). So, assuming that the atmospheric conditions remained constant during the time of the calibration, the relationship “ I_2/I_1 ” can be written as

$$\frac{I_2}{I_1} = \frac{S_2'/S_2^{std}}{S_1'/S_1^{std}}$$

Limitations

Due the nature of the calibration work (that requires stable atmospheric conditions, and very long trips between the both light sources sites), there was only a well-succeeded calibration data available (the night of 10/17/97).

The irradiance of the roving light is measured in the same way the irradiances of the *near* and *far sites*, by the use of the “blue” and “green” CCDs. In our calibration shift, we tried to avoid the use of the neutral density filters in front of the roving light when displacing it from the *far site* to the *near site*. The dynamic range of the used CCDs is just of 256 levels of gray. So the non-use of the neutral density filter required some CCD exposure time compensation, that must be performed *in loco* by a second person at the CCD site, that complicates the calibration procedure.

For these reasons, there was a further effort for the characterization of the relationship “ I_2/I_1 ” directly, by a photometric measurement of the light emitted by the light bulb used. However, to the present data analysis, it was used the only calibration data available, assumed representative even for the irradiance data acquired several months later.

The CCD “bad pixels” determination

In CCD cameras not all pixels work evenly, and so there are “bad pixels”. These pixels are characterized by the non-linearity of the electrical charge accumulated on the pixel with the time of exposure. The signal on these pixels results to be more dependent of other

parameters, such as the temperature of the CCD element. For this reason, CCDs for astronomical purposes are cooled to negative temperatures.

In our darkframe set of data it was verified that, basically, the values of accumulated charge for the bad pixels always increase with the exposure time. The “normal” pixels, instead, kept their “pedestal” values (with a typical fluctuation around this value), independently of the exposure time considered.

We used the increase of charge with time of exposure, present in our darkframe set of data, in order to discriminate the bad pixels for both CCDs. Using our darkframe set of data (took with several exposure times, in different occasions), first it was tagged the pixels that, in some darkframe, presented the pedestal value^{viii} + 2 times the typical fluctuation around this value. Following was performed an analysis in each of these “suspected” pixels: basically, their values were correlated with the exposure time of the different set of darkframes. If there was some kind of correlation (such as a clear increased of the pixel value with the exposure time), these pixels were considered as “bad pixels”.

This method was automated, due the large number of “suspicious” pixels to be analyzed, and also in order to be easily applied to any generic CCD. For this procedure, the characterization of the bad pixels is provided for the parameters of the own CCD under analysis, so being avoided the use of arbitrary cuts.

Cut Parameters

As a matter of fact, some of the bad pixels in our darkframe files showed a discrete rise with the exposure time, almost covered up by the typical fluctuation around the pedestal values. To these cases, it was adopted the criteria where a threshold valued of the “correlation coefficient” (in the plot “pixel charge value” vs. “darkframe exposure time”) was chose.

To the determination of this “threshold value”, it was made use of the decrease of the charge values in the “suspicious” pixels that sometimes showed up. It was assumed that a decrease trend was due solely due statistical fluctuations. In the selection criteria developed, it was considered as “normal” pixels all pixels that presented a correlation coefficient constrained between a range of values. The lower bound was set the most negative correlation coefficient value that occurred in the sample; correspondingly, the upper bound was set as its (symmetrical) absolute value (Figure 5).

In a more general criteria adopted, it was demanded that the root mean square of the “suspicious” pixels around the pedestal value was constrained around a typical value presented by pixels that had a correlation coefficient next to zero (*i.e.*, to darkframe pixels that presented the charge value disconnect with the exposure time). This was the final criteria adopted in our study, being the correlation coefficient value criteria just used if necessary .

^{viii} taken as the mean value of all the pixels in every darkframe file.

	CCD A (“blue”)	CCD B (“green”)
Total number of darkframe files	24	29
Total number of “suspicious” pixels	2809	7816
Total number of discriminated bad pixels ^{ix}	2313 (3% of all)	1570 (2% of all)

Table 1: Partial totals resultant from the selection process of the bad pixels.

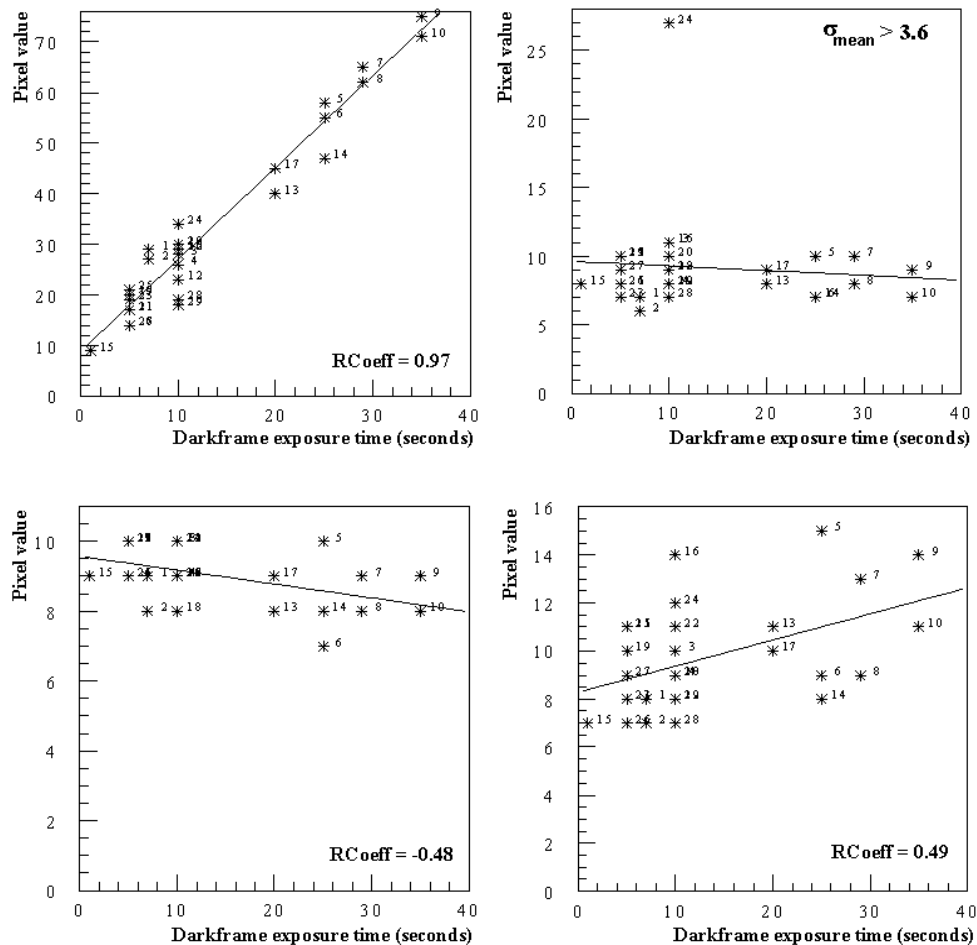


Figure 5: Some examples of how the dependence of the pixels values with the exposure time, presented in our darkframe set, was used in the selection of the bad pixels (regarded to the CCD B). Above, to the left: example of bad pixel where the recorded value had a clear dependence with the exposure time. Above, to the right: example of a bad pixel where the typical fluctuation around the pedestal values resulted greater than the value assumed as the “threshold”. Below, to the left: pixel that presented the most negative correlation coefficient, effect assumed the statistical fluctuation (this pixel was considered “normal”). Below, to the right: example of bad pixel where the value of the correlation coefficient was just above the “threshold value”, as showed before.

^{ix} In the CCDs used, the frames had 242 rows by 324 columns.

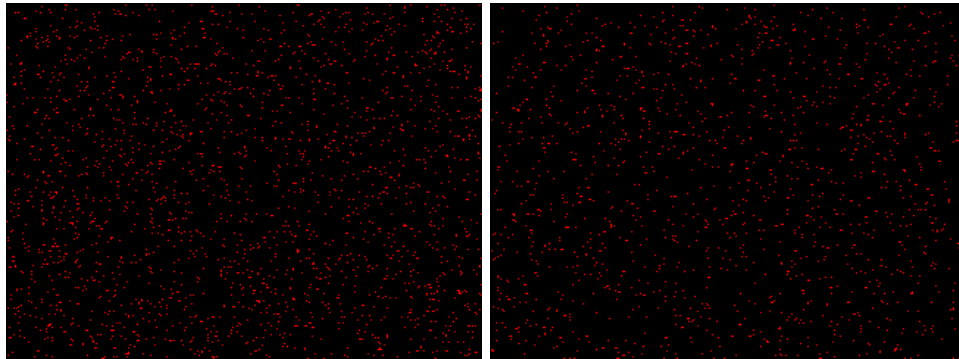


Figure 6: Bad pixel “map”, discriminated for the CCD A (blue) and CCD B (green). Note that the bad pixels are distributed uniformly on both CCD areas.

With the bad pixels identification, we could “clean” (remove) them from the images. In our analysis it was chose the replacement of each bad pixel value, by a mean value obtained from the 8 neighboring pixels. This number was changed when the bad pixel was near the image edge, or near other bad pixels (Figure 7).

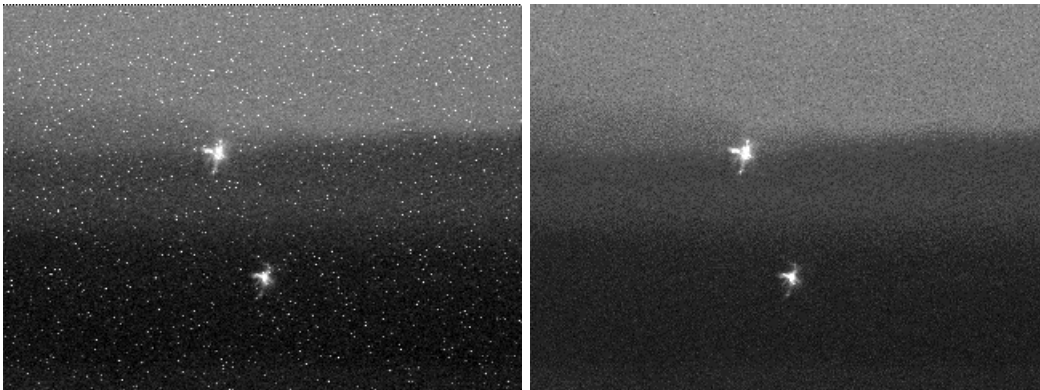


Figure 7: Example of bad pixel removing (CCD A, 02/11/97). Both pictures were changed for a better illustration. The leftmost picture is the “original”, clearly showing the bad pixels scattered on image. The rightmost picture was “cleaned” frame, being the bad pixels replaced by the mean value of the neighboring pixels.

The background subtraction

To a proper evaluation of the signal recorded in each bulb light spot, it is necessary characterize the background contribution, mainly due the CCD pixels charge pedestals and the recorded background light collected by the lens.

Usually we can assume the background on the CCDs as a constant value. Nevertheless, especially near full moon nights, the terrain profile focused by the CCD field of view appeared tenuously in our frames (as showed in Figure 7). In these cases the background could not be characterized as a constant value, and this non-uniformity must be accounted in some way.

Two different background subtraction were tried: by the use of “constant valued background”, and by the use of a “generic background”, obtained by inverse Fourier transform filtering.

The subtraction of a constant valued background

By this method, the background value is assumed as the mean value of all pixels of a particular image. In our study almost all the pixels in the bulb light recording have their value next to the background value, as the light bulb spotlight areas are very small respect the total picture area.^x

The subtraction of a constant value obtained was made for each pixel. However, for a safe background characterization, it was not used just the mean value obtained over the picture. Over this mean value is also calculated the root mean square of all pixels on the picture, and the background is assumed as the mean value of all pixels added to the root mean square of the pixels deviation multiplied by a scalar.

The value of this scalar was obtained by a semi-subjective (*ad hoc*) evaluation. In this present work, the final constant valued background was assumed as $\langle pixels \rangle + 3.5 * \sigma_{pixels}$, as it provided the best individualization of the spotlights recorded in each frame (as it will be discussed ahead).

^x For the same reasons, the root mean value deviation of the pixels, considering a particular frame, is close to the root mean value of the same “cleaned” (without bad pixels) frame. So, in order to save CPU time, in this analysis it was used the root mean deviation obtained with the raw CCD picture.

The subtraction of a generic background obtained by inverse Fourier transform filtering

In nights near the full moon the terrain profile appeared subtly in the CCD frames. In these frames, the “background” value for the part concerned to the sky was somewhat higher than the part concerned to the ground. As the sky area covered a large fraction of the frame, the total “constant valued” background of these photos resulted higher. This fact resulted an underestimation of the spotlight due to the *near site* bulb light, as the “background” in that part of the picture was lower.

For these cases it was tried a reconstruction of a “mean background”, just using the lower order frequencies of the CCD frames obtained by a Fourier transform process. By this process, the original image was transformed to the Fourier frequency domain, and then reconstructed (by inverse Fourier transform) only with the lower order frequencies.

It will not be exposed here the bidimensional Fourier transform in detail, as it can be found in complete references^{xi,xii}. It will just be exposed some of the difficulties regarded the choose of the filtering parameters, as applied in the present study.

The Bidimensional Fourier transform

The Fourier transform of the image in the Figure 7 (without the bad pixels) is showed in Figure 8. In a Fourier transform of a “real” image like the CCD pictures, all the “transformed” values will be complex numbers in the frequency domain^{xiii}. In Figure 8, not only the displayed image is altered for a better illustration, but also what is really being displayed is the complex number “module” of each frequency.

Following the bidimensional Fourier transform, there was the filtering of the high and medium frequencies (by a “low-pass” filter). The “filtered” transform is then reconstructed, through inverse Fourier transform.

Both processes (Fourier transform and inverse transform) are very CPU consuming, what constrained this method to just a selected set of the data.

^{xi} “Numerical Recipes in Fortran 77”. Cambridge University Press (1992).

^{xii} Rafael C. Gonzalez and Richard E. Woods, “Digital Image Processing”. Addison-Wesley Pub Co (1992).

^{xiii} In the bidimensional Fourier transform, each element of the resulting matrix represent a frequency.

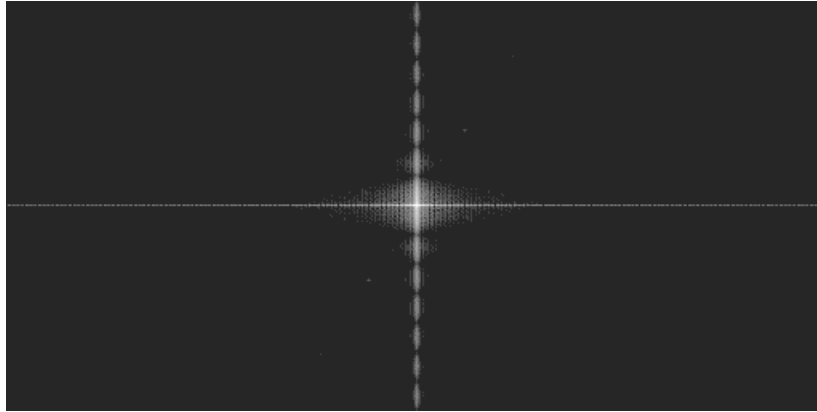


Figure 8: The Fourier transform of the picture displayed in the Figure 7 (without bad pixels). The present image is changed to this illustration - the lower frequency terms (next to the origin) are dominant, and by far larger than the other terms. Note that the dimension of the displayed image is different of the original image size; this is a characteristic of the FFT (*Fast Fourier Transform*) algorithm.

The “low-pass” filter

The proper selection of a “cut threshold” for the low-pass filter is the most delicate step concerning the background characterization.

Similarly as what happens with a unidimensional Fourier analysis, the first order terms refers to the constant background value of the picture. The following terms include the fundamental harmonics. As we include more terms in the reconstruction, we have harmonics related to higher frequencies that correspond to the picture details.

However, just the reconstruction with the first harmonics cannot provide a good representation of a generic background. As in the case of the unidimensional Fourier analysis, the image borders (considered as “discontinuities”) will be badly reconstructed by the inverse Fourier transform that follows. Despite, the lower order harmonics that comes next can provide a significant percentage of the signal on the pixels, and the use of a short range of low-order harmonics would imply in a non-representative image even for the background. On the other hand, as we increase the number of frequencies, the reconstructed image will approach the original image.

Despite, in our particular case, the lower-order harmonics are prone to add up constructively in the spots region, especially if the pixel values on the spots are substantially higher than the background. So a subtraction of such a background will lead to a signal loss in the spots region.

The reconstruction of a generic background for the image presented in Figure 7, with the application of several low-pass thresholds, is shown in Figure 9. It was defined as a “low-pass” filter a mask centered in the origin (the fundamental frequencies) of the Fourier transformed image. Only the frequencies that were inside the “cut threshold” radius were preserved; the remaining frequencies were set to zero.

As the Fourier/inverse Fourier transforms are CPU consuming, in the present study the process of the subtraction of “generic background” was just applied in nights that were 5 days before, and 5 days after, the full moon (where the background terrain profile was prone to appear; Figure 12 and Figure 13). The “cut threshold”, for the low-pass filter used in this study, was chose as “8” (that was verified to provide a good description of the reconstructed background).

Even when the “original” images was subtracted from the generic background obtained by Fourier transform filtering, there was a remaining “DC” component. This “DC” component was accounted as a constant valued leftover, and was also subtracted from the “original” images.

It was latter verified that, for a better spot identification (that will be explained next), it should be subtracted a second constant valued background that, likely what happened in the case of the constant valued background, accounted for the pixels fluctuation around the mean value of the all pixels in the original images^{xiv}.

In this study it was chose, *ad hoc*, that the generic background would consist of three components: the inverse Fourier transformed (filtered) background + the remaining “DC” component (from the difference of the “original” image and the obtained generic background) + 1.5 times the root mean square deviation around the mean value of all pixels of the “original” image. This latter addition not only provided a better spot identification but also, in the case of nights without moon, returned spot intensities values close to the values obtained by the application of a constant valued background method.

^{xiv} After the subtraction of the generic background obtained by inverse Fourier transform filtering, we can think about the final result as better suited for the application of an algorithm similar the “constant valued background method”.

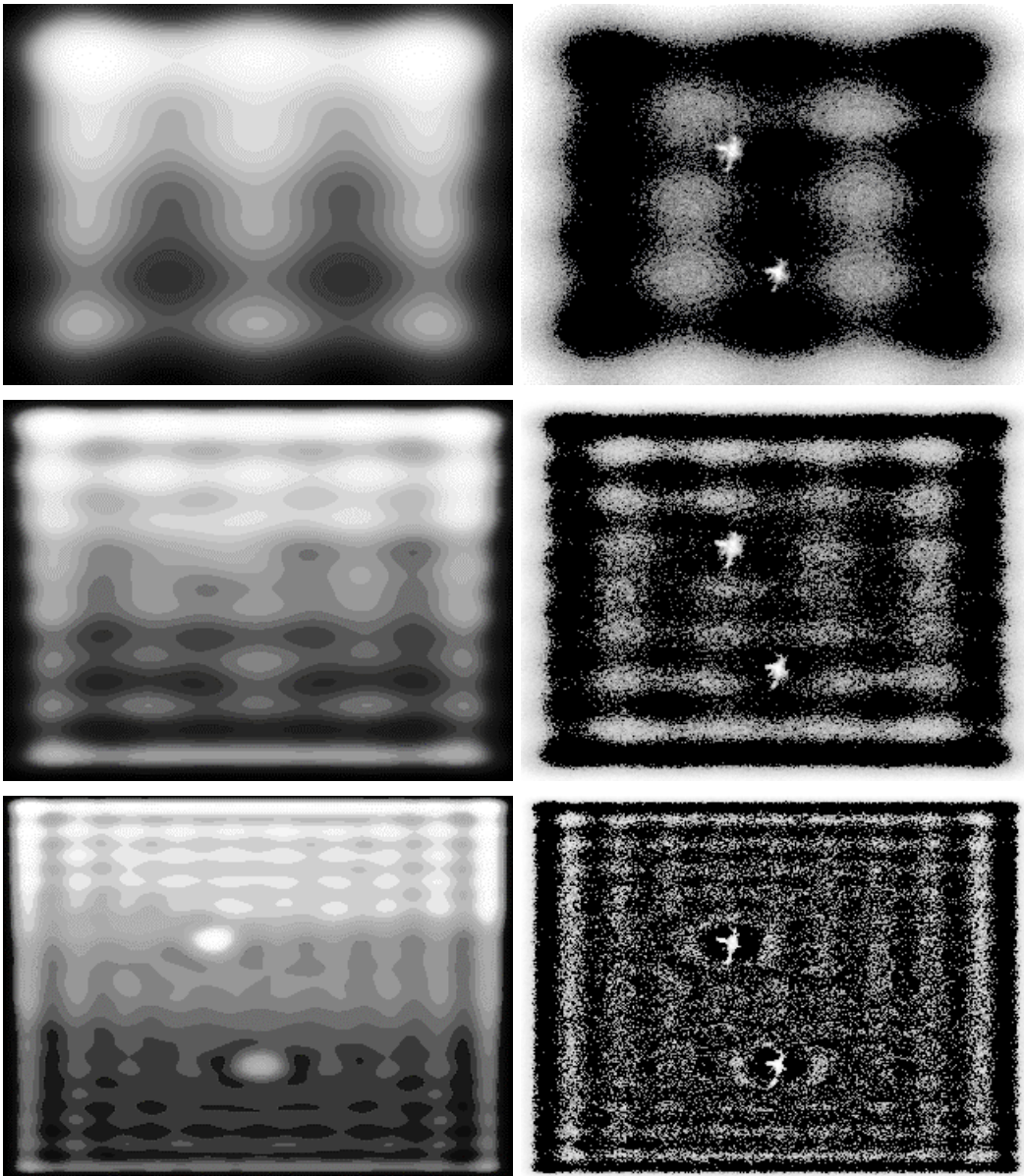


Figure 9: Inverse Fourier transformed images obtained from Figure 7, reconstructed after the application of low-pass filters (on the right, from top to below, filters of factor “4”, “8” and “16”). On the left we have the corresponding subtraction of the original images and the reconstructed ones (all images here were altered for a better illustration). Note that the borders were just better reconstructed as the number of frequencies increased.

The automatic spots identification

Our sample of raw data consisted in about 14 thousand frames to be analyzed. In some occasions, the spot positions in the frames changed for some handling of the CCD box. However, more important in what concerns this study, sometimes we didn't have both spots present in the image (usually for some local obscuration by the bulb light site). In order to didn't be trick by a non-existent spot, it was devised an algorithm to determinate the spot positions automatically, as the input of data frames was streamed into the analysis code.

The automatic detection was also necessary due some overcomes during the winter too: due the low temperatures on the site, the Wratten filters, made in a substrate of gelatin, crinkled. As the low temperature conditions persisted, the spot images obtained under these conditions resulted irregular and progressively different from night to night (this is the case presented in Figure 7, shot during February of 98).

The spot identification algorithm was split in two parts. In the beginning it was looked for bunches of 9 pixels above the value stated as a "background"^{xv}, being demanded that the central pixel of the 3x3 square mask, as well all the surrounding 8 pixels around, were above the background. In the end of this step, the detected bunches of 3x3 masks were merged if they shared common pixels among them.

In the following step, each bunch was "enlarged". Each pixel of each bunch was checked for an enlargement, being a 5x5 square mask placed on it. Whichever pixel of the 5x5 mask that was above the background and didn't belong to the bunch of pixels under analysis was merged to the bunch, and was later subjected to the same enlargement algorithm. The process was repeated until there was no further pixels to be merged to the bunch under analysis.

Again, after we have all bunches enlarged, a final check was made looking again for common pixels being shared among different bunches of pixels. Bunches of pixels that shared pixels among themselves were again subjected to a merging.

For a definitive spot identification, it was used several of the fixed parameters of the experiment arrangement in the final identification of bunches of pixels (as the distance, in pixels, between the *near* and *far site* spots, as well the "vertical distance" we estimated between the spots). If the algorithm found very large dimensions for the spots (being in rows, or being in columns units), the spot was dismissed, for safety.

When at least one of the spots were not positively identified, the positions of both spots would remain indeterminate. In order to provide the identification of the existent spot, it was used the last spots positions determinate in the previous frame. If the previous spot position was not valid, the indetermination remained until there were at least two spots identified in the subsequent frames.

^{xv} It's worth to remind that the "background", obtained assuming a constant valued background, or by the inverse Fourier filtering method, were slightly different.

Besides the process was CPU time consuming, this algorithm provided to be reliable. As a subproduct, not only the mask of pixels that composed the spots, but also the integrated sum of the pixels in the spot, was effectuated in the process.

In full moon nights, the constant valued background method didn't lead to a good spot identification. Typically, in our sample of data, the values of the pixels inside the spots were slight higher the mean background. Even a slightly change of the background value could alter too much the spots characterization. A better description of the background, as provided with the inverse Fourier filtering method, minimize this effect.

When looking for spots using the generic background provided by the inverse Fourier transform filtering method, the borders values of the background image was badly reconstructed, what resulted be a source of difficulties (Figure 9). In the implementation used, the borders were simply discarded, being however necessary a definition about the effective extent of a "border".

In this work, for the border characterization, we used the subtracted result from the original image and the "generic background" image. On the borders, the subtraction resulted "high" values. As we stepped towards the image center, the subtraction yielded "lower" numbers, until the characteristic "almost zero" numbers, expected for in our case.

A mean value, of all pixels, of this subtraction resulting image was calculated, and assumed as the "characteristic value" waited after the subtraction. For each row, and for each column, taken from the borders towards the image center, it was verified if any of its pixels exceed the value of 2 times the mean value of all pixels of the subtracted image. When such a row, or such a column was found (all of its pixels were lower than 2 times the mean value of the subtracted image), the row, or column, was assigned as the first "valid" borders for our purposes. All the pixels of the former rows, and of the former columns, were set to the mean value of the pixels of the subtracted image.

Further, in the case of the generic background provided by the inverse Fourier transform filtering, an inconvenience came from the "senoidal pattern" presented in the subtracted image. Regarded the spot identification procedure the "ripple", when high, resulted in an identification of a false spot (Figure 10).

To overcome this difficult, in the spot identification were excluded any spots, of bunches of pixels, that were spread around a large area in the image. Besides, if there were too many spots identified in the image, automatically the process was repeated with the generic background increased by 10%. This background increasing was repeated until a "reasonable" number of spots were identified, or until some limit for the number of repetitions was reached.


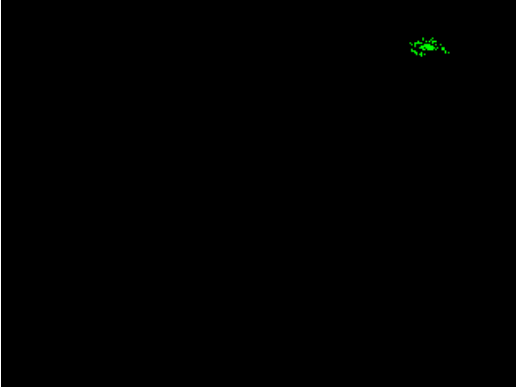

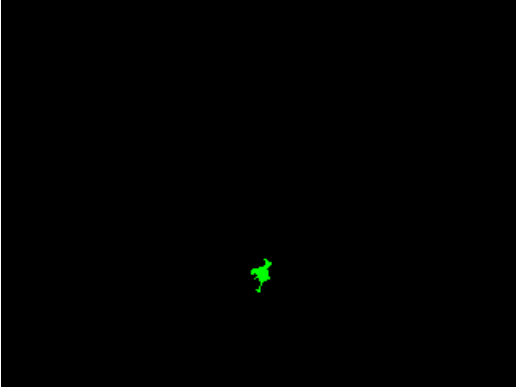
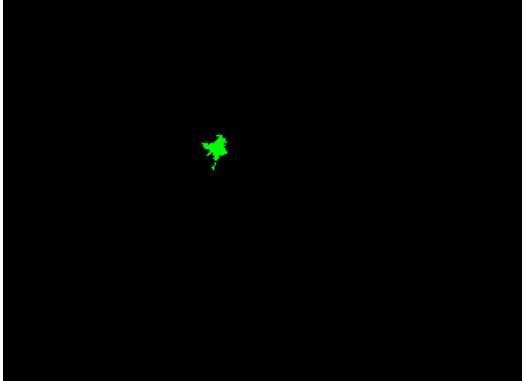
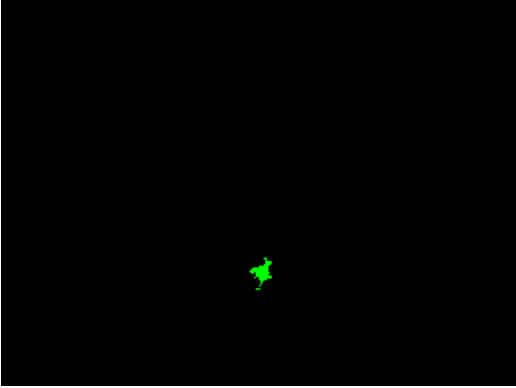
<p><i>CCD A, a044-22g.fits (image altered for a better display, without bad pixels) - after full moon night</i></p>	<p><i>Spot identification after the background subtraction by inverse Fourier transform filtering: spot 1 (ripple - spurious)</i></p>
	
<p><i>Spot identification after the background subtraction by inverse Fourier transform filtering: spot 2 (far site)</i></p>	<p><i>Spot identification after the background subtraction by inverse Fourier transform filtering: spot 3 (near site)</i></p>
	
<p><i>Spot identification after the background subtraction of a constant valued background: spot 1 (far site)</i></p>	<p><i>Spot identification after the background subtraction of a constant valued background: spot 2 (near site)</i></p>
	

Figure 10: Spot identification in a frame without the terrain profile, with the two methods described.

General CCDs characteristics over the measurement period of data taking

In Figure 12 to Figure 15 are presented some general CCDs characteristics (as the mean value of the pixels of the images^{xvi}, and the root mean square of these pixels mean values^{xvii}). The plots of the mean value of all pixels and the pixels root mean square around the mean value show, roughly, a summarized description of the quality of the measurements.

As a matter of fact, the referred plots helped to individualize some “accidents” during the data taking, like filter displacements^{xviii}. Additionally, some atypical frames could be also identified, and so eliminated of our analysis (Figure 11).

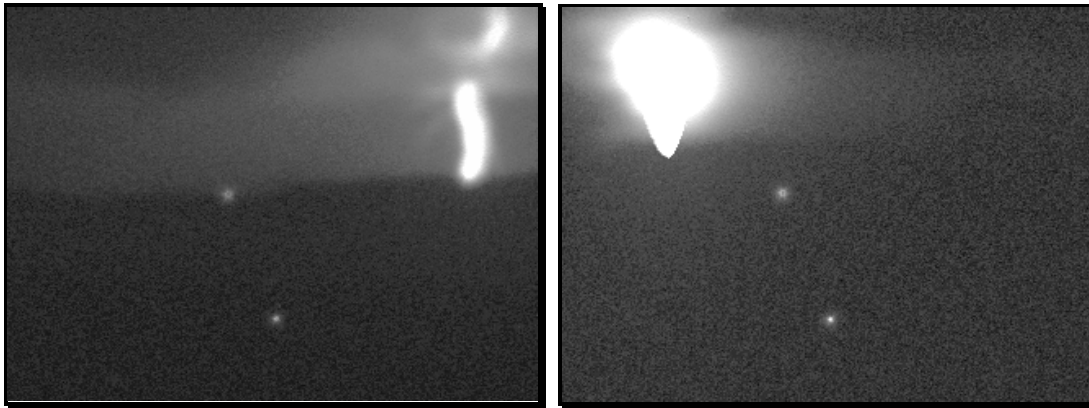


Figure 11: frame *a155-023d.fts* (with a lightening) and *a126-04j.fts* (where the moon was caught inside the field of view of the CCD).

In all plots shown, the error bars refer to the respective value deviation when the set of 10 images (shot in a predefined hour of the night) was considered. This is especially true for the plots of the mean value of all pixels, and the pixels root mean square around the mean value.

As shown is Figure 14 and Figure 15, usually the deviation present in pixel root mean square values is somewhat low inside the sets of 10 frames shot in a particular night hour. This fact will be used as quality criteria for the final data selection.

^{xvi} Referred to the average over the 10 images, shot in predefined hours of the night

^{xvii} the same as above.

^{xviii} Periods were the CCDs pixel mean values assumed exaggerated high values. These periods were disregarded in our analysis.

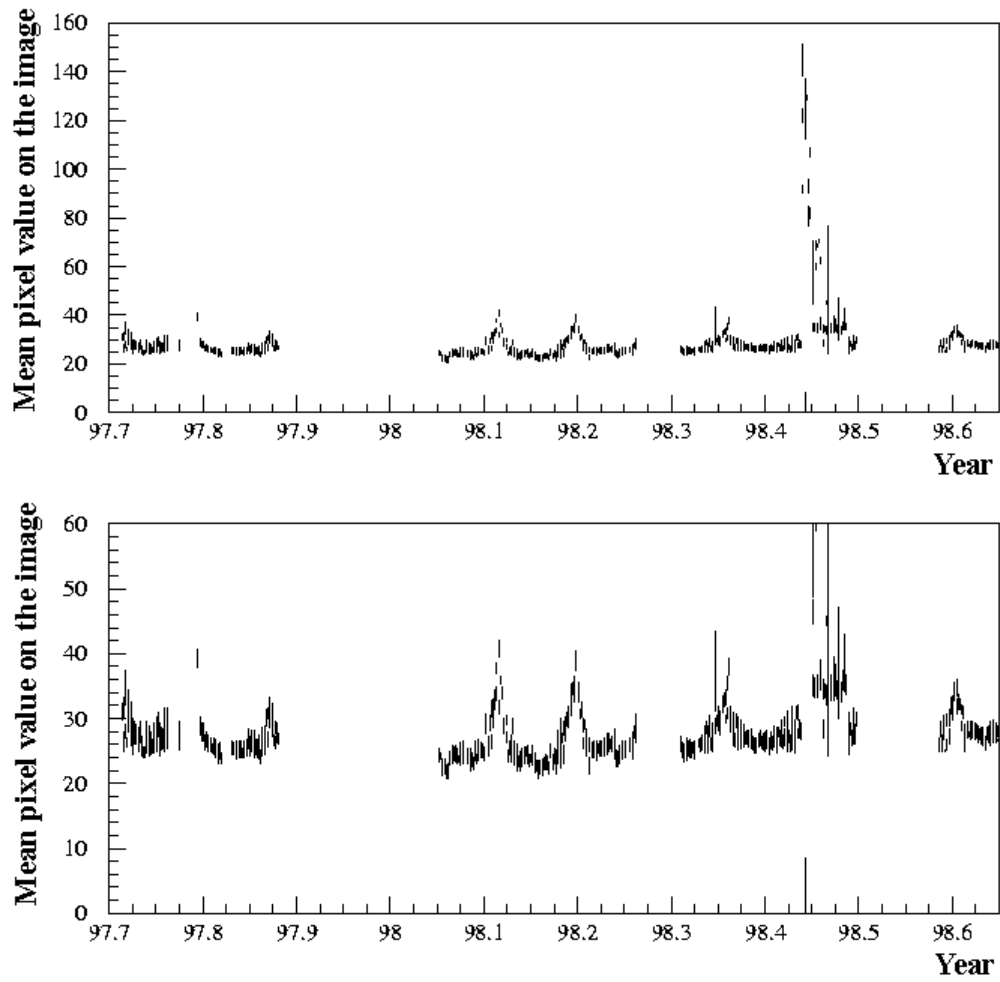


Figure 12: Mean value of all pixels, for the sets of frames of the **CCD A** (in the plot below, we have an enlargement of the y-axis scale). It was verified that the “peaks” refer to the full moon nights.

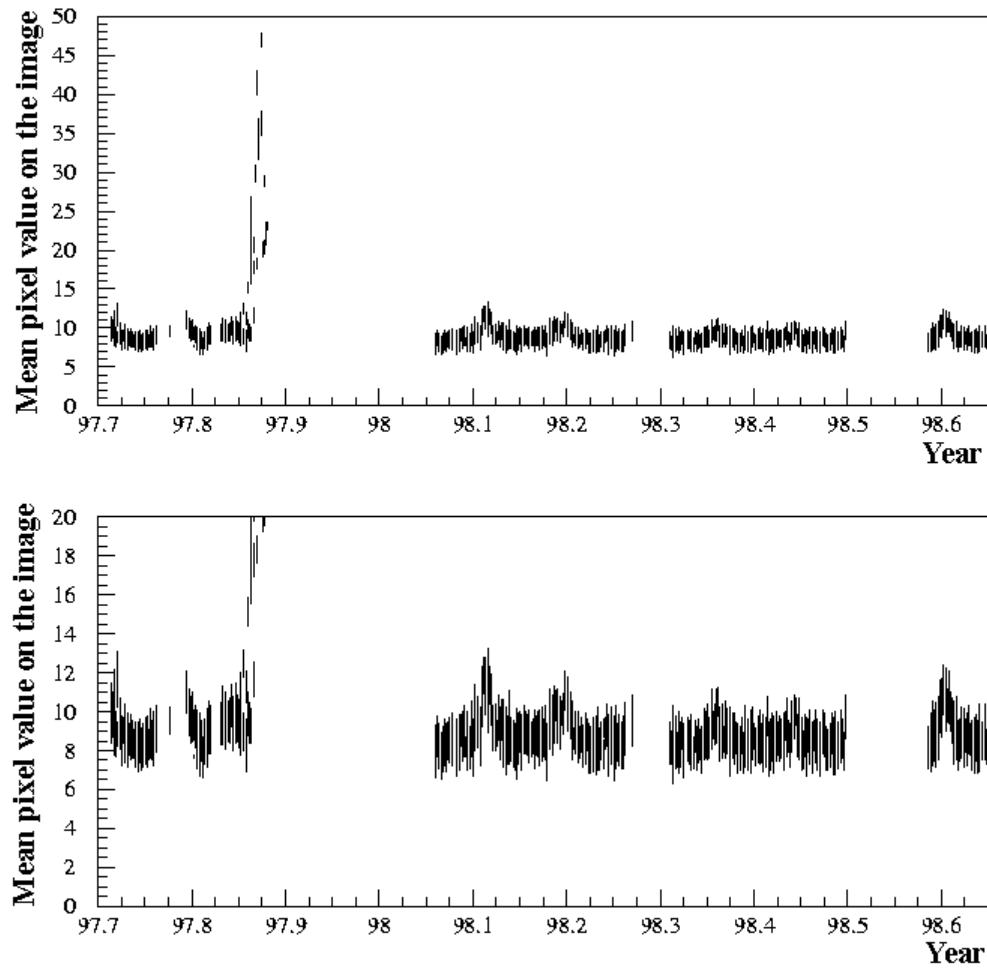


Figure 13: Mean value of all pixels, for the sets of frames of the **CCD B** (in the plot below, we have an enlargement of the y-axis scale). It was verified that the “peaks” refer to the full moon nights.

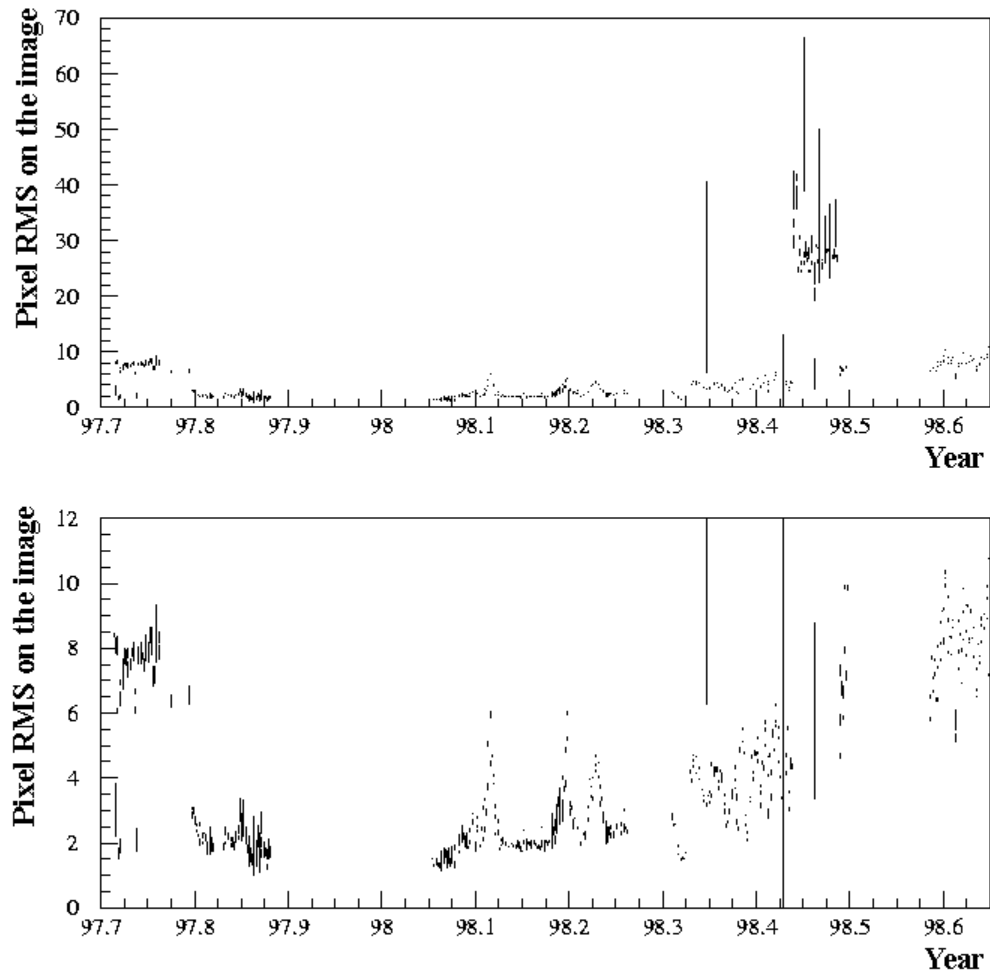


Figure 14: Pixels root mean square (around the mean of all pixels of the images), for the sets of frames of the **CCD A** (in the plot below, we have an enlargement of the y-axis scale).

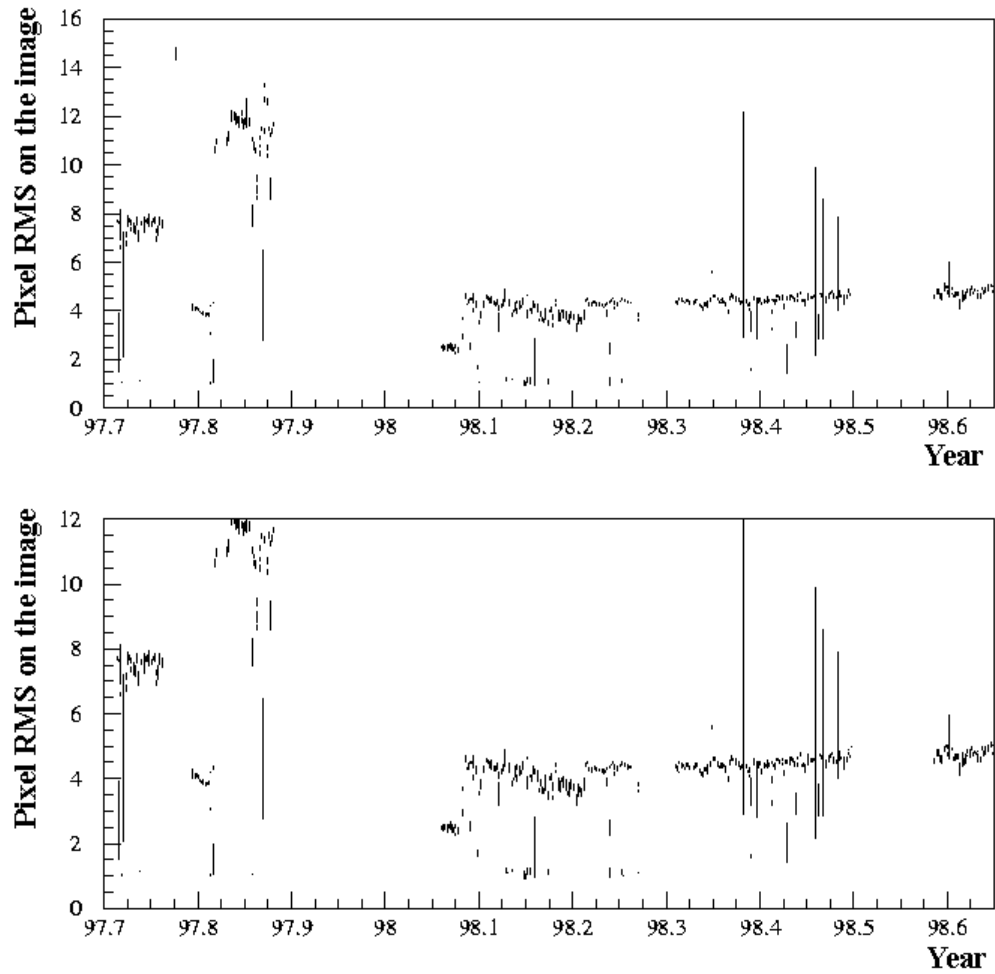


Figure 15: Pixels root mean square (around the mean of all pixels of the images), for the sets of frames of the **CCD B** (in the plot below, we have an enlargement of the y-axis scale).

The near light bulb voltage monitoring

The light bulb placed on the *near site* was powered by a set of car batteries charged by solar panels. By the use of timers, the light was kept turned on during part of the night.

In order to monitoring the batteries voltage decrease, it was installed a *logger* that sampled the batteries voltage at every hour.

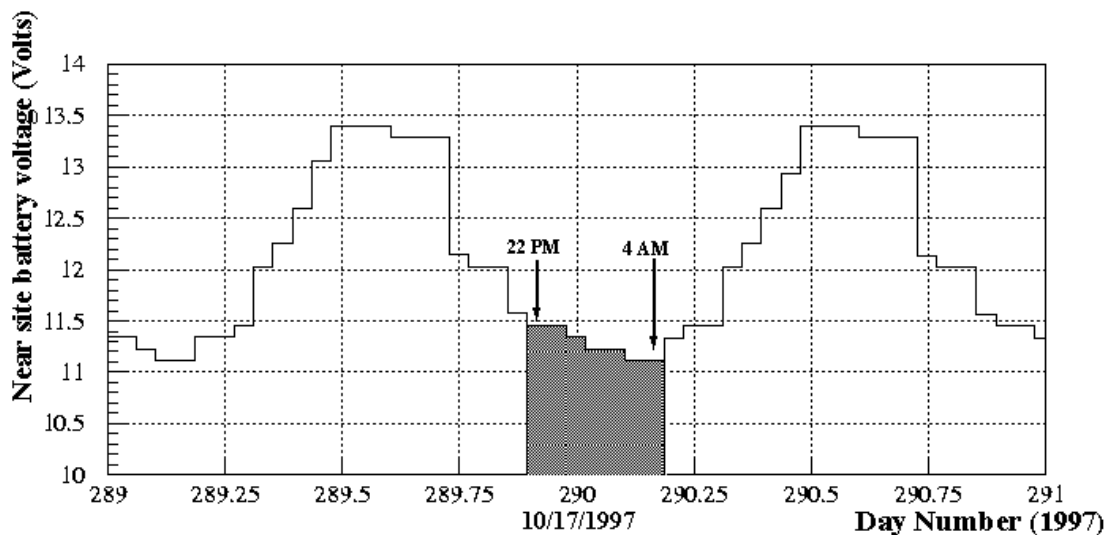


Figure 16: A typical voltage fluctuation, in the batteries that powered the near site bulb.

Besides the large variation presented during a full day period, during the time of CCDs data acquisition the variation was about 0.5 over 11.5 Volts (Figure 16). However, it is commonly assumed that the light output of a light bulb varies (roughly) with the voltage powered to 2.7. So, even a 0.5 Volts variation could mean about 12% of the near light total yield.

A monitoring of the battery voltage was particularly important during the winter months. On these months bad weather, cloudy skies and snow deposited on the solar panels prevented a full recharge of the batteries.

A log of the battery voltages during the winter period is showed on Figure 17. We can see several days where the batteries were somewhat discharged during the CCD data acquisition period. These days should not be considered on the final data appreciation (as, for example, the nights between 02/08 and 02/11/98), but we will avoid establishing cut criteria at this point.

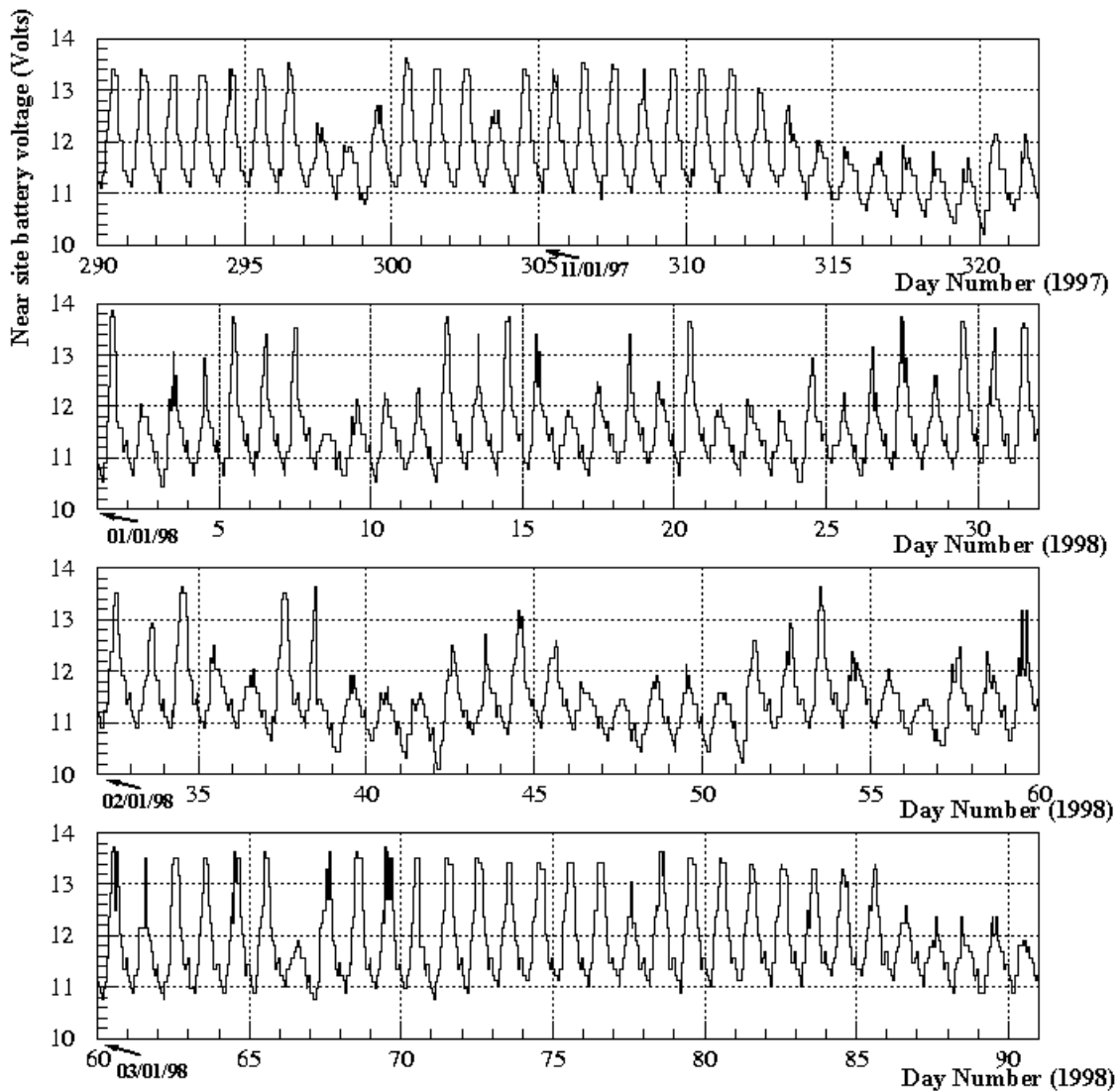


Figure 17: Voltage log, of the batteries of the near site bulb, during the winter period.

It is worth to note that the "loading" part of the voltage curves (during the morning) can vary greatly from day to day. However, during the data acquisition period, the 0.5 Volts variation was the rule for most of the nights.

With the voltage log, it is possible to implement some kind of correction for the total light output. In this work, however, the effect of the battery discharge will be considered of "secondary order".

Calibration procedures

The night of 10/17/97 was the only night where the calibration procedure resulted successful.

The calibration shift began at 12h40 AM and finished at 2h53 AM. On the following tables it is shown the light intensities measured, be by the application of the “constant valued background” method, as well by the application of the “inverse Fourier transform filtering” method.

CCD A (“blue”)					
Intensities obtained with the “constant valued background” method					
	number of measurements	Mean intensity on the CCD spot (pixel counts)	Error		Time of exposure
			RMS	Error on mean	
Roving (calibration) light (<i>near site</i>)	16	1374.76	± 350.34	± 87.59	1 sec
Roving (calibration) light (<i>far site</i>)	12	445.38	± 53.64	± 15.48	10 secs
Light bulb present on the <i>near site</i>	20	862.40	± 62.91	± 14.07	10 secs
Light bulb present on the <i>far site</i>	13	766.82	± 123.63	± 34.29	10 secs

CCD A (“blue”)					
Intensities obtained with the “inverse Fourier transform filtering” method.					
	number of measurements	Mean intensity on the CCD spot (pixel counts)	Error		Time of exposure
			RMS	Error on mean	
Roving (calibration) light (<i>near site</i>)	16	1276.66	± 311.88	± 82.97	1 sec
Roving (calibration) light (<i>far site</i>)	12	425.66	± 54.33	± 15.68	10 secs
Light bulb present on the <i>near site</i>	20	912.19	± 59.57	± 13.32	10 secs
Light bulb present on the <i>far site</i>	13	723.60	± 107.09	± 29.70	10 secs

Table 2: Calibration night summary for CCD A (“blue”)

CCD A (“green”)					
Intensities obtained with the “constant valued background” method					
	number of measurements	Mean intensity on the CCD spot (pixel counts)	Error		Time of exposure
			RMS	Error on mean	
Roving (calibration) light (<i>near site</i>)	14	1581.54	± 449.81	± 120.27	1 sec
Roving (calibration) light (<i>far site</i>)	12	604.04	± 107.58	± 31.06	10 secs
Light bulb present on the <i>near site</i>	9	1335.44	± 110.05	± 36.68	10 secs
Light bulb present on the <i>far site</i>	9	1128.36	± 220.80	± 73.60	10 secs

CCD A (“green”)					
Intensities obtained with the “inverse Fourier transform filtering” method.					
	number of measurements	Mean intensity on the CCD spot (pixel counts)	Error		Time of exposure
			RMS	Error on mean	
Roving (calibration) light (<i>near site</i>)	14	1521.04	± 429.83	± 114.87	1 sec
Roving (calibration) light (<i>far site</i>)	12	601.13	± 96.22	± 27.78	10 secs
Light bulb present on the <i>near site</i>	9	1358.11	± 109.56	± 36.52	10 secs
Light bulb present on the <i>far site</i>	9	1098.44	± 206.72	± 68.90	10 secs

Table 3: Calibration night summary for CCD B (“green”)

We can see that the error, associated to the measured intensities, are quite large. This fact can result from atmospheric turbulence (always present, especially in the case of a horizontal path, near the ground), or to some intrinsic imprecision of the CCDs measurements.

With the intensities measured in the calibration night, we can estimate the mean free path, for both wavelengths CCD ranges, present in that night. From our former description of the calibration of the measurements (see section “Description of the employed analysis and calibration”), we have (for a same light source in the *near e far sites*):

$$I_1 = I_2 \quad \text{and} \quad \lambda = \frac{(r_2 - r_1)}{\ln\left(\frac{S_1^{std}\left(\frac{r_1^2}{r_2^2}\right)}{S_2^{std}\left(\frac{r_1^2}{r_2^2}\right)}\right)}$$

Making use of the numbers yield by the tables above, and remembering that the roving light intensity, when placed in the *near site* **was not** attenuated by the use of a gray (neutral) filter, we have (normalizing the exposure time in the frames):

CCD A:		
	$\lambda = 34.26 \text{ km}$	(obtained by the application of the “constant valued background” method)
	$\lambda = 35.25 \text{ km}$	(obtained by the application of the “inverse Fourier transform filtering” method)

CCD B:		
	$\lambda = 40.83 \text{ km}$	(obtained by the application of the “constant valued background” method)
	$\lambda = 42.52 \text{ km}$	(obtained by the application of the “inverse Fourier transform filtering” method)

Furthermore, making use of the values obtained in the calibration night, we can determinate the ratio I_2/I_1 , required for the data reduction of the remaining nights.

Remembering that the *near site* bulb was attenuated by a X8 factor by the use of a gray (neutral) filter, but the roving light intensity, when placed in this site, **was not** attenuated by such a filter, we have (normalizing the exposure time in the frames):

CCD A:		
	$I_2/I_1 = 3.431$	(obtained by the application of the “constant valued background” method)
	$I_2/I_1 = 2.973$	(obtained by the application of the “inverse Fourier transform filtering” method)

CCD B:		
	$I_2/I_1 = 2.765$	(obtained by the application of the “constant valued background” method)
	$I_2/I_1 = 2.558$	(obtained by the application of the “inverse Fourier transform filtering” method)

... different if it was assumed the previously known nominal values for the bulbs (20 Watts for the light bulb in the *near site*, and 35 Watts for the light bulb in the *far site*), but also incommoding next to each other (the basic assumption was that the mean free paths measured by CCD A and CCD B would be different, because they referred to distinct wavelengths).

The error propagation in the measurements

It was made an evaluation about how such a large relative errors, as in the case of our measured intensities, would affect the mean free path determinations.

Remembering that we can assume the light bulb distance errors as negligible, and the quantities in the evaluation (S_1 , S_2 e I_2/I_1) can be assumed disconnected, we have, from the error propagation theory:

$$(\sigma_\lambda)^2 = \left(\frac{\partial\lambda}{\partial S_1}\right)^2 (\sigma_{S_1})^2 + \left(\frac{\partial\lambda}{\partial S_2}\right)^2 (\sigma_{S_2})^2 + \left(\frac{\partial\lambda}{\partial I_2/I_1}\right)^2 (\sigma_{I_2/I_1})^2$$

$$\left(\frac{\partial\lambda}{\partial S_1}\right) = \frac{-\lambda^2}{(r_2 - r_1)S_1}; \quad \left(\frac{\partial\lambda}{\partial S_2}\right) = \frac{\lambda^2}{(r_2 - r_1)S_2}; \quad \left(\frac{\partial\lambda}{\partial I_2/I_1}\right) = \frac{\lambda^2}{(r_2 - r_1)I_2/I_1};$$

and so,

$$\sigma_\lambda = \frac{\lambda^2}{(r_2 - r_1)} \sqrt{\left(\frac{\sigma_{S_1}}{S_1}\right)^2 + \left(\frac{\sigma_{S_2}}{S_2}\right)^2 + \left(\frac{\sigma_{I_2/I_1}}{I_2/I_1}\right)^2}$$

As we can see, the error in “ λ ” is proportional to “ λ^2 ”. This is a drawback, because our intention is to measure long mean free path in the atmosphere.

Taking $\frac{\sigma_{S_1}}{S_1} = \frac{\sigma_{S_2}}{S_2} = 0.05$, and assuming $\frac{\sigma_{I_2/I_1}}{I_2/I_1} = 0.10$ (after the numbers we have from the calibration night), we have that

$$\sigma_\lambda = 0.12 \frac{\lambda^2}{(r_2 - r_1)} \cong 3.5 * 10^{-3} \lambda^2$$

So, for an expected mean free path evaluation of 40 km, we mean an error in the measurement of ± 5.6 km.

Results

The mean free paths obtained, as well the expected errors, are shown from Figure 18 to Figure 24.

Talking about the CCD A data set, there was a displacement of the Wratten filter in the “*day number*” 159 of 1998, being this displacement repaired only on “*day number*” 177 of 1998. The data collected between the “*day number*” 213 and 236 is very different from the data obtained before, with the appearing of a large amount of bad pixels, different from the ones previously detected. It was assumed here that the CCD A characteristics deteriorated in the period that preceded this data taking. These both set of data were also discarded.

About the CCD B data set, from “*day number*” 303 of 1997 until the restart of the data taking in 98 the spots in the CCD frames have a large number of *overflow* pixels, what indicates a bad intervention in its objective diaphragm. Besides, from “*day number*” 310 of 1997 until the restart of the data taking in 98, there was a displacement of the infrared cutoff filter of the CCD B. All this period of data was then discarded.

In the analysis presented in this work, each set of frames, taken in predefined hours of the night, were summed up and than divided by the total number of images of the set. On this “mean” frame was made the background subtraction and spot identification. However, just were subjected to this analysis sets of frames that:

- have at least 8 images in the set;
- were similar to each other (the mean value of all pixels of each image, when averaged over the total number of images present on the set, could not present a variation greater than the arbitrary value of 3 pixel counts - Figure 12 and Figure 13);
- behave similarly to each other (the root mean square value of all pixels around the mean value of each image, when averaged over the total number of images present on the set, could not present a variation greater than the arbitrary value of 1 pixel count - Figure 14 and Figure 15);
- presented positively identified, simultaneously, the both spots correspondent to the *near e far site*.

Following the methodology employed in this analysis, the images shot 5 days before, or 5 days after a full moon had their background estimated by the inverse Fourier transform filtering method. On the other days, the constant valued background method was applied on the data.

The relationship “ I_2/I_1 ”, settled in the calibration night of 10/17/97 and applied to all set of data until the finish of the experiment data taking, was chose as the value yielded by the “constant valued background” method ($I_2/I_1 = 3.431$ for CCD A, and $I_2/I_1 = 2.765$ for CCD B).

It was used, as “valid” data in our analysis, the data took when the Wratten filters were crinkled (from the beginning of 98 to the “day number” 77 of 1998). The resulting light spots on CCDs were irregular in shape, and spread on a large area of the CCD element. Just after the “day number” 77 of 1998 (03/18/98) this overcome was corrected, being the Wratten filters enclosed a sheet of thin glass. Thus, the spots intensity determination is expected to be worse, when compared to the spot intensity reduced in other periods.

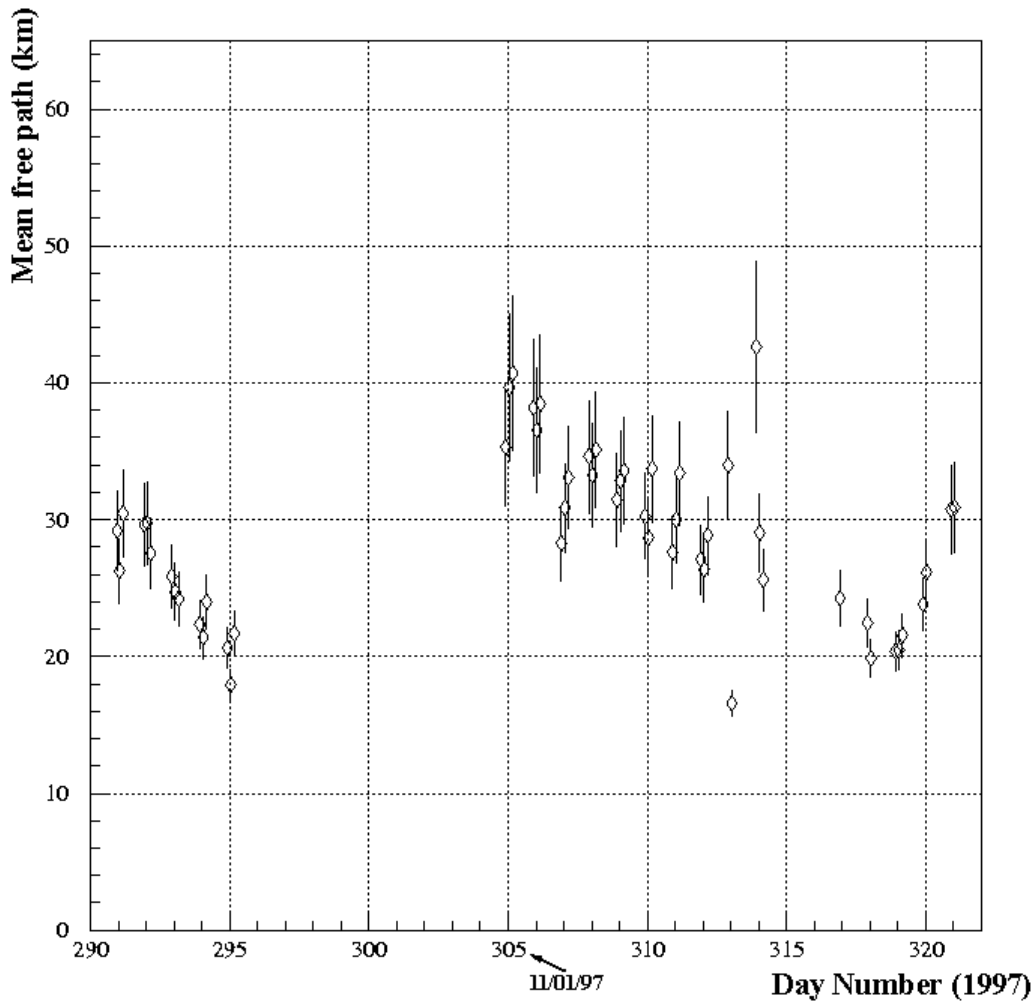


Figure 18: Atmospheric mean free paths measured with the CCD A (“blue”) device, between 10/17/97 and 10/22/97, and between 11/01/97 and 11/11/97.

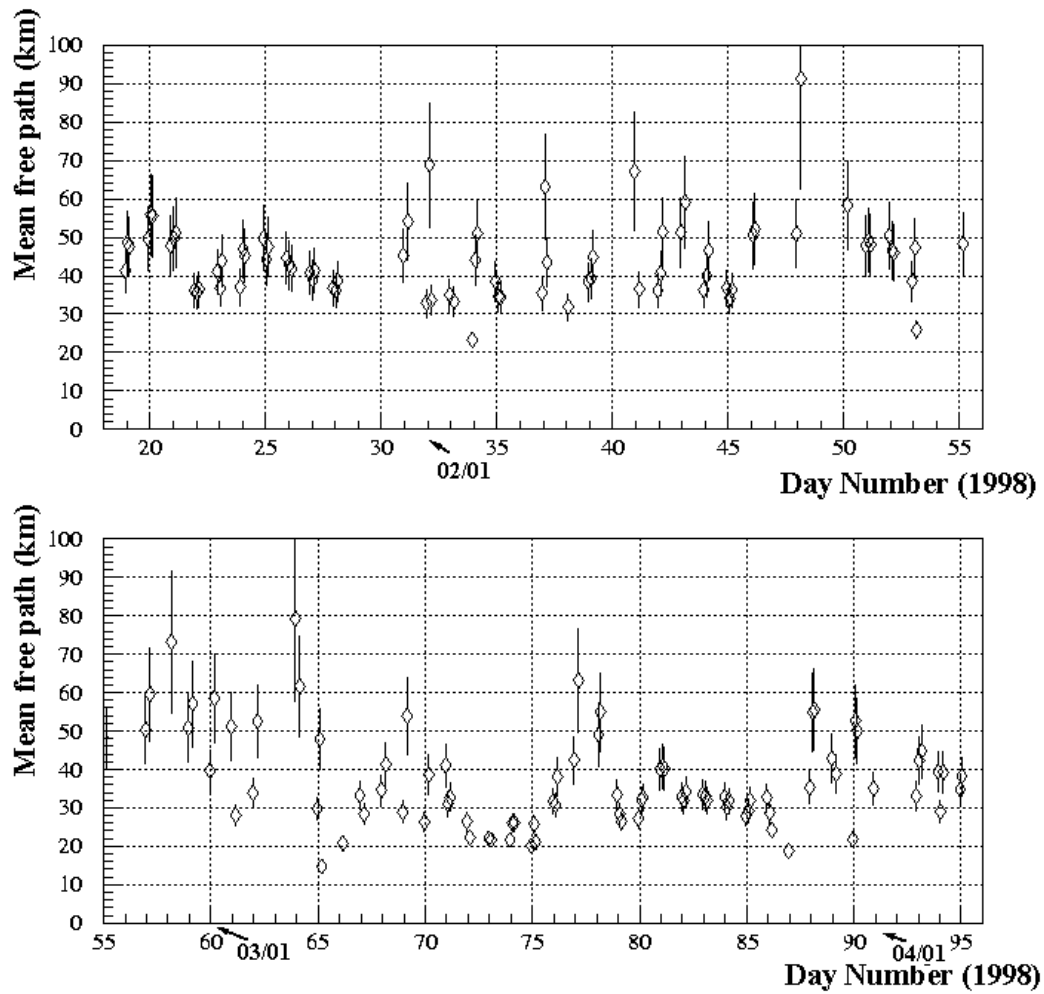


Figure 19: Atmospheric mean free paths measured with the **CCD A** (“blue”) device, between 01/18/98 and 04/05/98.

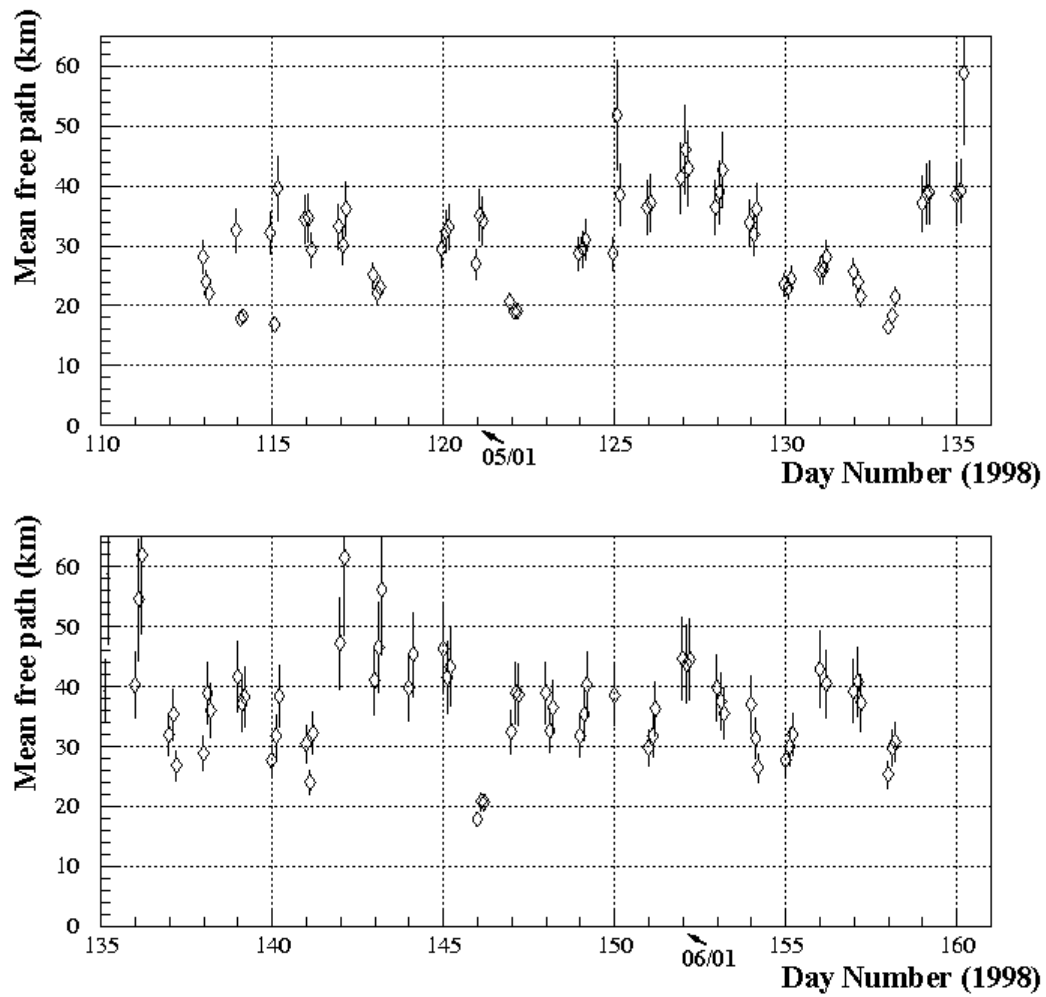


Figure 20: Atmospheric mean free paths measured with the **CCD A** (“blue”) device, between 04/22/98 and 06/08/98.

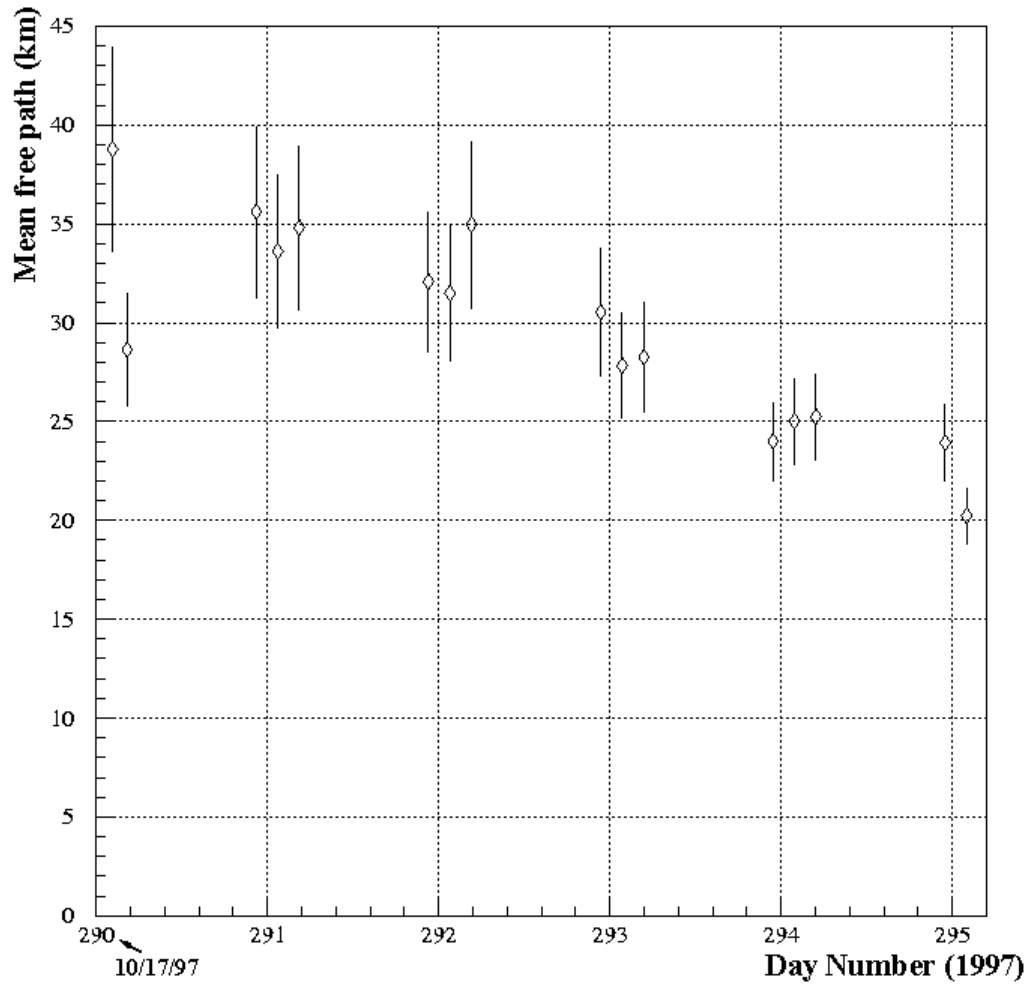


Figure 21: Atmospheric mean free paths measured with the **CCD B** (“green”) device, between 10/17/97 and 10/22/97.

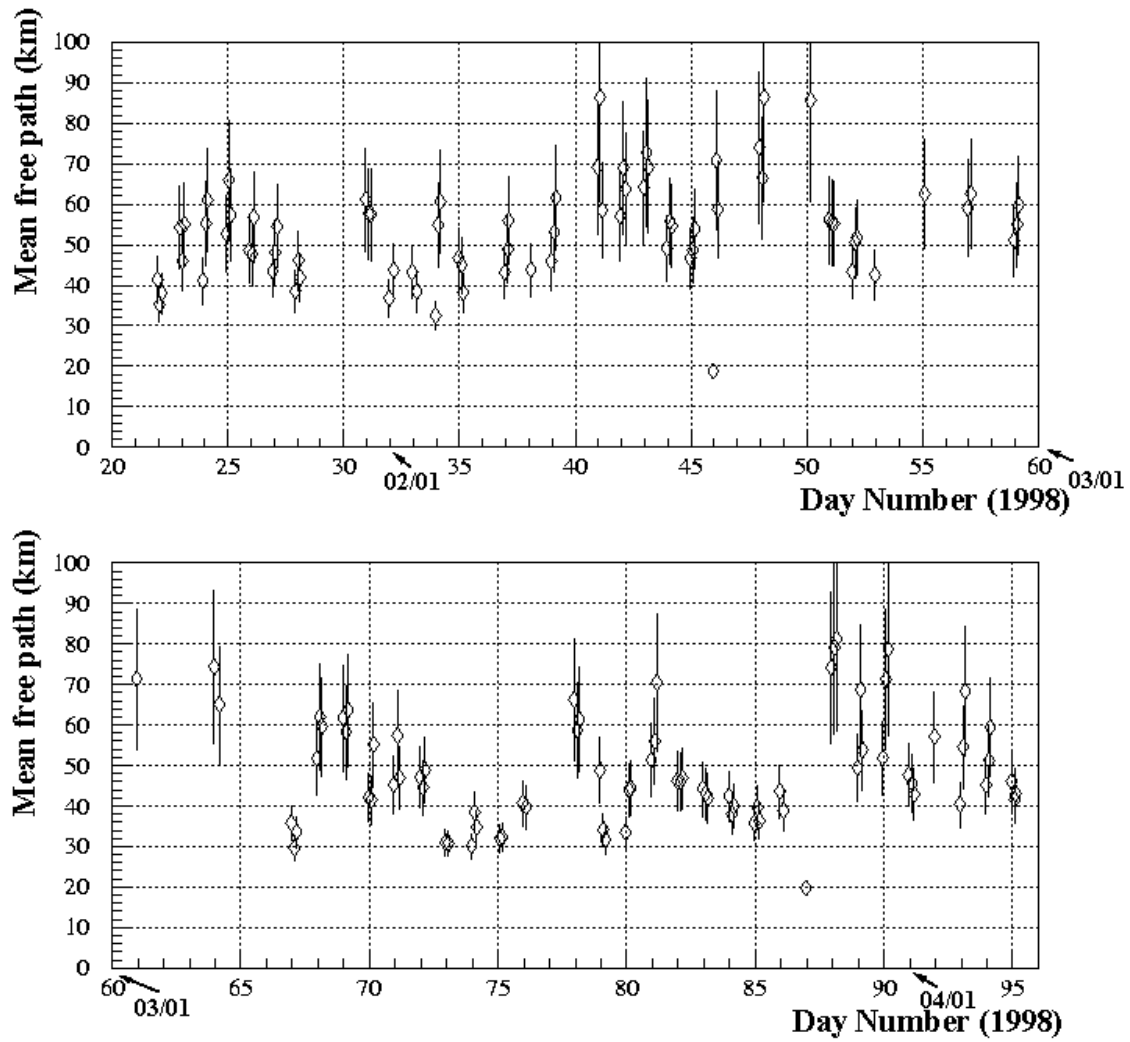


Figure 22: Atmospheric mean free paths measured with the CCD B (“green”) device, between 01/18/98 and 04/08/98.

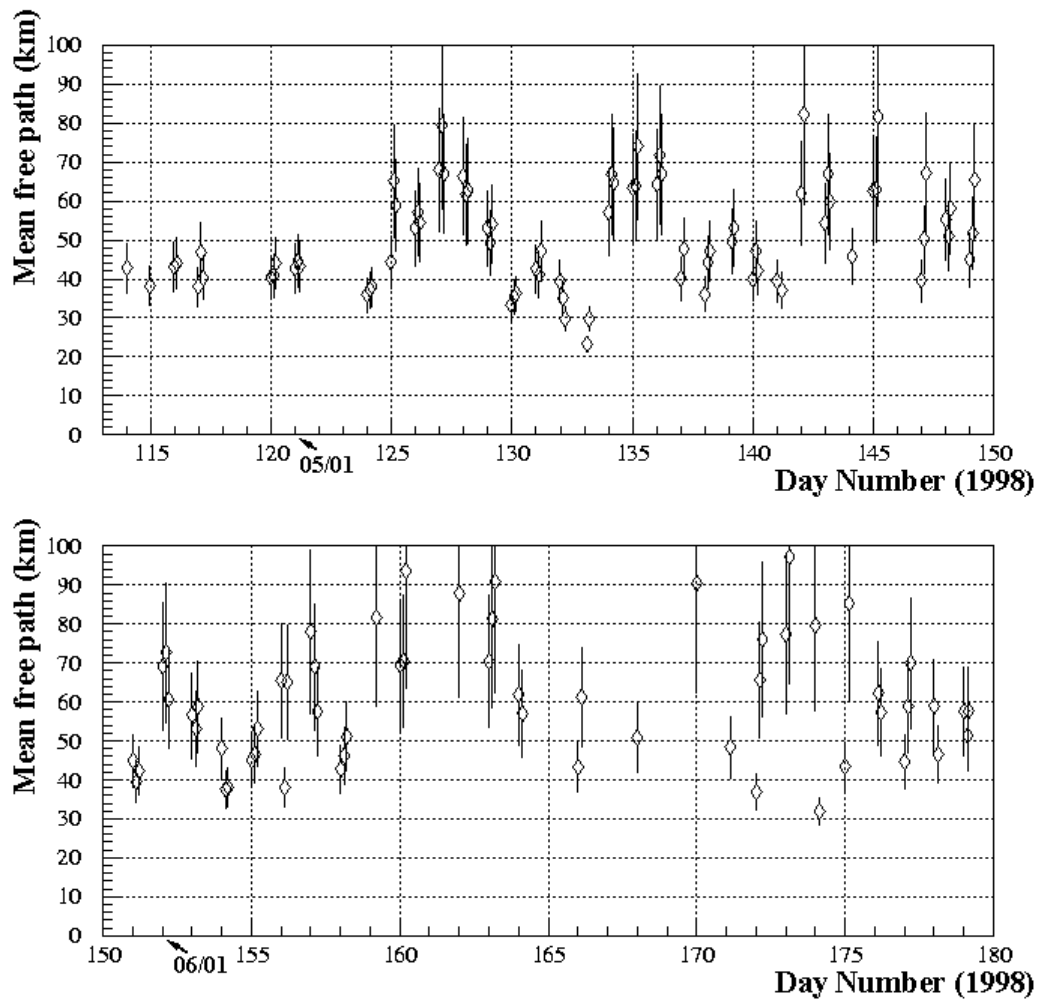


Figure 23: Atmospheric mean free paths measured with the **CCD B** (“green”) device, between 04/22/98 and 06/29/98.

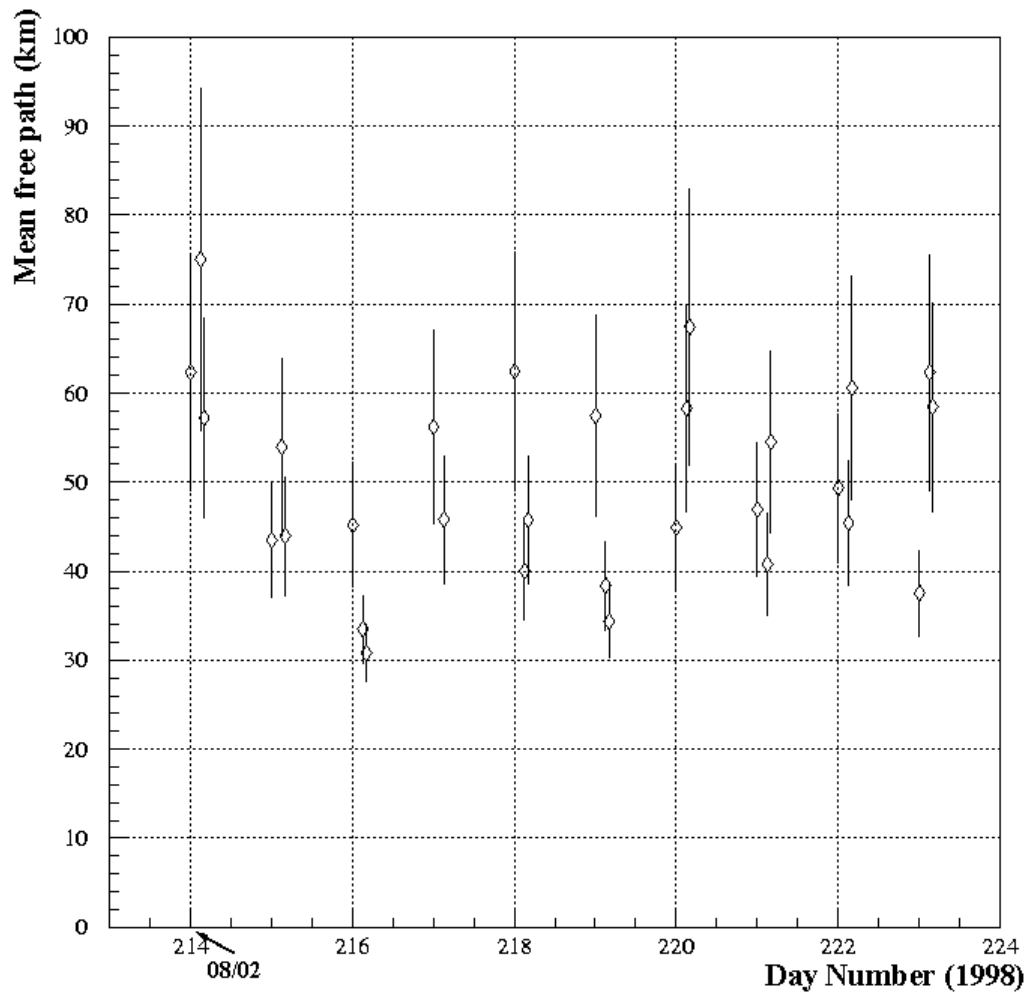


Figure 24: Atmospheric mean free paths measured with the **CCD B** (“green”) device, between 08/01/98 and 08/12/98.

Analysis and Discussion

The presented results show some ambiguity referred the expected results. Following the MODTRAN estimate for a clean atmosphere of “desert” type, it is very unlikely that the mean free paths measured by the CCD A and CCD B could be equivalent (Figure 25 e Figure 26).

The mean free path measured by the CCD B (centered on the “green” wavelength, and thus close to the valued estimated by the naked eye) are high, even in atmospheric conditions assumed “rare” (Table 4).

In the case of a hypothetical atmosphere without aerosols, only the scattering due molecules (Rayleigh scattering) would produce a maximum *Meteorological Range* value of 250 km. Remembering the relationship between the mean free path in the visible and the *Meteorological Range*, given by

$$(\text{Meteorological Range}) = \frac{3.912}{\beta_{tot}} = 3.912 * \lambda \text{ (km)}$$

we would expect, as a “maximum mean free path” limit for the CCD B, the improbable value of 65 km. We have in our data values higher than this limit.

Perhaps we shouldn’t use the calibration values obtained in the night of 10/17/97. As presented in the error bar evaluation, even small a changing in the apparatus would produce large deviations in our numbers (as a matter of fact, the range of values that S_1/S_2 can assume for “reasonable” mean free path values is very narrow).

Some explanation for the large mean free paths measured can be found in the basic assumption of the uniformity of the atmosphere. An investigation on some very high numbers obtained, or even negative mean free path values (not showed) reveal an obscured spot light in the *near site* (a negative mean free path would reflect as a “light amplification” in our data).

Besides, the used CCDs, available to amateur astronomers, sometimes showed some fluctuations among the frames shot inside the same predetermined period of night. Better CCDs would minimize the short dynamic range we were subjected too.

However, the main suspect for the high numbers obtained refers to the efficiency of “*Infrared Cutoff*” filter used. A “leakage” of infrared light into the CCDs would explain why the CCD A and CCD B mean free paths finished, in the end, to yield similar mean free paths estimates.

It can be seen a very high degree of correlation between the data from CCD A and CCD B. This correlation indicates that, in principle, the method works. Moreover, the nights with uncorrelated data still require a better understanding.

Atmospheric conditions	“Meteorological Range” (Visibility)
“Pure” air (only molecules, without aerosols)	277 km ($\beta_{sc} = 0.0141 \text{ km}^{-1}$)
“Exceptionally clear” conditions	from 20 km, to greater than 50 km
“Clear” conditions	from 10 to 20 km
Light haze	from 4 to 10 km
Haze	from 2 to 1 km
Light fog	from 1 to 500 m

Table 4: Typical *Meteorological Range* values, referred to the atmospheric conditions.

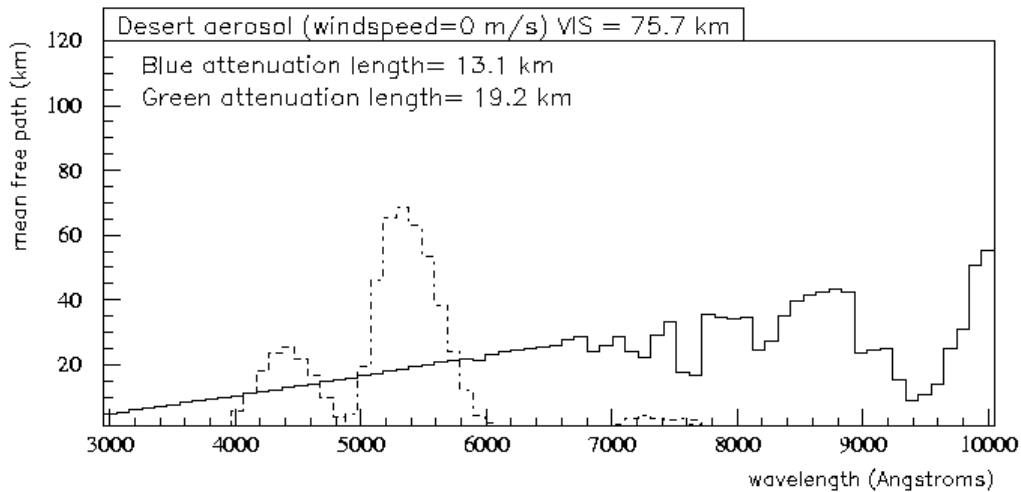


Figure 25: Mean atmospheric mean free path, expect by the “blue” and “green” CCDs, under the “desert” atmospheric conditions (windspeed = 0 m/s; “midlatitude winter” latitude range and ground level 1.5 km above sea level). The dash and dash-dotted lines refer to the spectral efficiencies (“CCD quantum efficiency” + “Kodak Wratten filter efficiency” + “Infrared Cutoff filter efficiency”) for the CCD chamber under evaluation.

Finally, there was two remaining sources of imprecision: the atmospheric turbulence near the level of the ground (perhaps the 10 seconds value, chose as the exposure time, was insufficient to average the scintillation of the light received), and the discharge of the battery that powered the bulb light in the *near site*. The voltage decrease that occurred during the night, recorded by a *logger* placed *in loco*, was not taken in account in this present study. An additional analysis work would be required to verify the proper behavior of our non-ohmic elements.

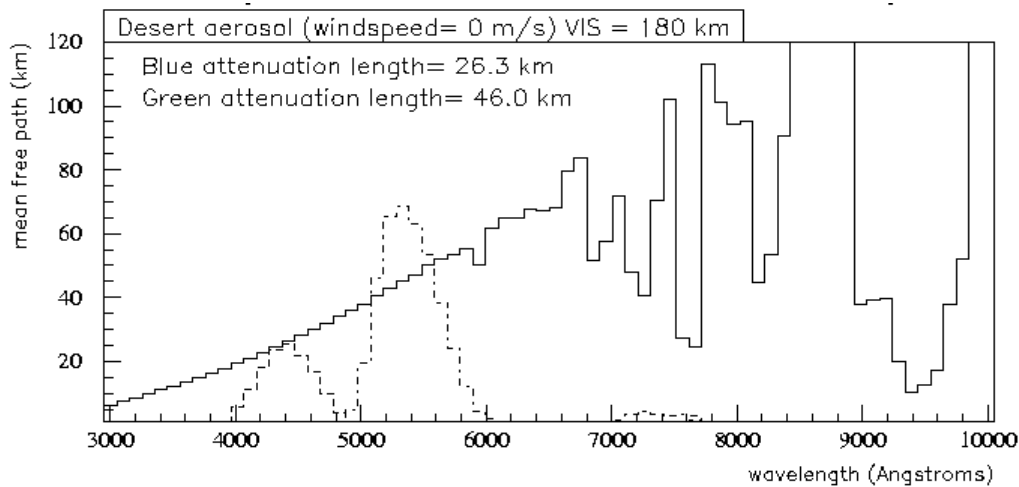


Figure 26: Mean atmospheric mean free path, expect by the “blue” and “green” CCDs, under the “desert” atmospheric conditions (windspeed = 0 m/s; “midlatitude winter” latitude range and ground level 1.5 km above sea level). We forced here an initial **Meteorological Range of 180 km** in the input too. The dash and dash-dotted lines refer to the spectral efficiencies (“CCD quantum efficiency” + “Kodak Wratten filter efficiency” + “Infrared Cutoff filter efficiency”) for the CCD chamber under evaluation.

Conclusion

The experiment resulted inconclusive referred a proper evaluation of the atmospheric mean free path for the northern site. However, the good correlation between the CCD A and CCD B measurements is very auspicious, and indicates that a further development of the method should be tried.

The large error bars present in the present evaluation could be greatly decreased through a more reliable photometry. CCD chambers that present a wider dynamic range, or that provide relative variations of about 5%, would bring the errors bars to a imprecision of ± 2.3 km, if its considered mean free paths of 40 km.

A proper verification of the spectral characteristics of the optical filters used was a detail that resulted of importance. A lot of effort was spent until some good understand of the apparatus characteristics, but apparently it’s not advisable to trust the manufacturer specs.

The non-uniformity of the atmosphere, as would be the “real” case to be found outdoors, produced some inconsistency among the reduced data. An interesting possibility would be a combination of the photometry of light sources near the ground with the photometry of stars. It would be worth to consider some LIDAR^{xix} evaluation too.

Finally, the problem of the calibration of the experiment have still to be better developed.

^{xix} Acronym for “Laser in Atmosphere Ranging”.